iScience

CellPress
OPEN ACCESS

Article

Loss of Fgf9 in mice leads to pancreatic hypoplasia and asplenia

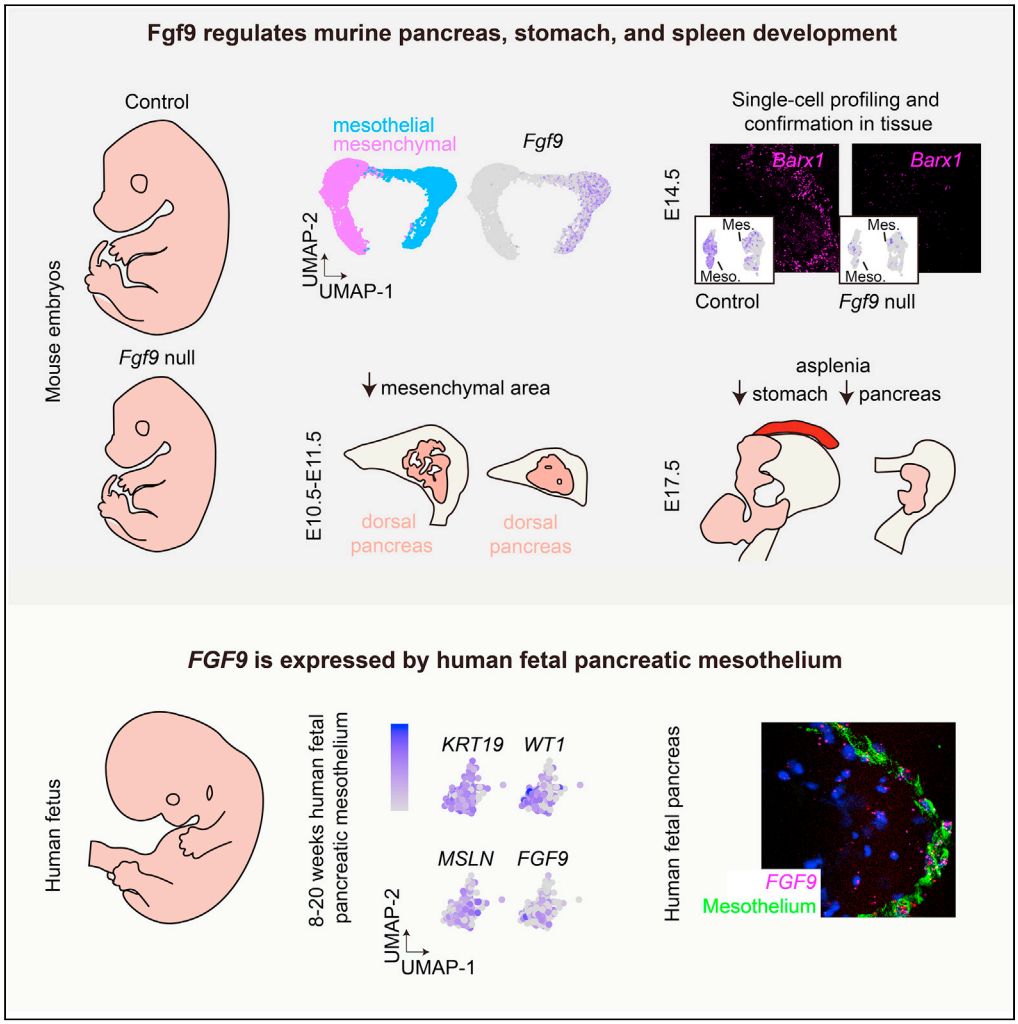

Sophie Patzek, Zhe Liu, Sean de la O, ..., Xiuqin Zhang, David M. Ornitz, Julie B. Sneddon

julie.sneddon@ucsf.edu

Highlights

In early mouse pancreas development *Fgf9* is expressed by mesenchyme and mesothelium

Global *Fgf9* knockout displays reduced pancreas and stomach size, complete asplenia

Transcriptional programs are perturbed in pancreatic mesenchyme on *Fgf9* loss

Expression patterns of *FGF9* and receptors are conserved in human fetal pancreas

Patzek et al., iScience *26*, 106500
April 21, 2023
https://doi.org/10.1016/j.isci.2023.106500

iScience

CellPress
OPEN ACCESS

Article

Loss of Fgf9 in mice leads to pancreatic hypoplasia and asplenia

Sophie Patzek,[1,2,3,4,5,7] Zhe Liu,[1,2,3,4,7] Sean de la O,[1,2,3,4] Sean Chang,[1,2,3,4] Lauren E. Byrnes,[2,3,4] Xiuqin Zhang,[6] David M. Ornitz,[6] and Julie B. Sneddon[1,2,3,4,8,*]

SUMMARY

Pancreatic development requires spatially and temporally controlled expression of growth factors derived from mesenchyme. Here, we report that in mice the secreted factor Fgf9 is expressed principally by mesenchyme and then mesothelium during early development, then subsequently by both mesothelium and rare epithelial cells by E12.5 and onwards. Global knockout of the *Fgf9* gene resulted in the reduction of pancreas and stomach size, as well as complete asplenia. The number of early Pdx1+ pancreatic progenitors was reduced at E10.5, as was proliferation of mesenchyme at E11.5. Although loss of Fgf9 did not interfere with differentiation of later epithelial lineages, single-cell RNA-Sequencing identified transcriptional programs perturbed upon loss of *Fgf9* during pancreatic development, including loss of the transcription factor *Barx1*. Lastly, we identified conserved expression patterns of *FGF9* and receptors in human fetal pancreas, suggesting that *FGF9* expressed by pancreatic mesenchyme may similarly affect the development of the human pancreas.

INTRODUCTION

Temporally and spatially coordinated epithelial–mesenchymal interactions are central to the development of the primitive gut tube endoderm and are necessary for the formation of functional organs of the gastrointestinal tract, including the pancreas. A comprehensive identification of the extrinsic signals that regulate pancreatic morphogenesis is crucial not only for understanding the fundamental mechanisms underlying developmental biology of the organ *in vivo*, but also for refining protocols to generate pancreatic tissues from pluripotent stem cells *in vitro* for physiology studies, disease modeling, and cell replacement.[1–12]

The development of the pancreas begins around embryonic day (E) 8 in the mouse, when secreted factors from the neighboring mesoderm and notochord specify the region of endoderm that will ultimately give rise to the pancreas.[13–16] Around E9, a group of loosely packed, spindle-shaped cells, collectively termed the mesenchyme, condense around the dorsal gut and facilitate the growth of the budding epithelium. The transcription factor Pancreatic and duodenal homeobox 1 (Pdx1) marks the earliest pancreatic progenitors that give rise to the pancreatic epithelium. Pdx1-expressing pancreatic progenitors proliferate from E9.5 to E12.5, followed by specification of the pancreatic lineages.

Early development of the dorsal pancreas and spleen occurs as a confluence within the dorsolateral mesentery of the stomach (or mesogastrium).[17–19] The putative splenic and dorsal pancreatic mesenchyme lies beneath a specialized, transient portion of the dorsal mesentery, termed the splanchnic mesodermal plate (SMP), which appears bilaterally around Pdx1+ epithelium and persists on the left side until about E11.5.[19,20] Inductive signals from the SMP are important for the appearance and condensation of underlying mesenchymal cells, which will themselves give rise to the spleen as well as the dorsal pancreatic mesenchyme around E10.5, and the SMP directs leftward growth of these organs. By E11.5, a primordial spleen is formed and is attached to the dorsal pancreatic primordium, with these organs lined by a mesothelial sheath that expresses Wilms' tumor 1 (WT1). Rotation of the stomach and leftward movement of the dorsal pancreas brings together the dorsal and ventral pancreatic buds, which fuse and grow along an axis perpendicular to the duodenum. Meanwhile, the spleen remains associated with the lateral stomach wall. As epithelial proliferation and branching morphogenesis proceeds, the pancreatic epithelium protrudes into the surrounding cap of mesenchymal cells. The rapid growth of the epithelium results in a

[1]Department of Cell and Tissue Biology, University of California, San Francisco, San Francisco, CA 94143, USA

[2]Department of Anatomy, University of California, San Francisco, San Francisco, CA 94143, USA

[3]Diabetes Center, University of California, San Francisco, San Francisco, CA 94143, USA

[4]Eli and Edythe Broad Center of Regeneration Medicine and Stem Cell Research, University of California, San Francisco, San Francisco, CA 94143, USA

[5]Division of Endocrinology and Metabolism, University of California, San Francisco, San Francisco, CA 94143, USA

[6]Department of Developmental Biology, Washington University School of Medicine, St. Louis, MO 63110, USA

[7]These authors contributed equally

[8]Lead contact

*Correspondence: julie.sneddon@ucsf.edu

https://doi.org/10.1016/j.isci.2023.106500

decreasing ratio of mesenchymal to epithelial cells across development, with rare mesenchymal cells present in the adult pancreas.[21]

Signals from the mesenchyme play a critical role in supporting survival, proliferation, migration, differentiation, and branching morphogenesis of the developing pancreatic epithelium.[22,23] The importance of mesenchyme in pancreatic development has been demonstrated by both physical and genetic population ablation approaches,[21,24] as well as deletion of mesenchymally-expressed genes such as NK3 Homeobox 2 (*Nkx3.2*),[17] Homeobox C6 (*Hox6*),[25] and PBX Homeobox 1 (*Pbx1*).[26]

Disruption of various mesenchymal paracrine signaling pathways has identified essential regulators of pancreatic epithelial growth and function, including Wnt, BMP, and TGFbβ.[27–33] In particular, FGFs have been well recognized as important mesenchymally-derived secreted factors essential to pancreatic organogenesis even before E12.[19,30,31,33–35] Previous work showed that *Fgf9* is expressed in the dorsal SMP, a transient structure that drives the appearance and condensation of the underlying mesenchymal cells to form the spleen and pancreatic mesenchyme between E9.5 and E11.5.[19,36] In addition to Fgf9, Fgf10 is expressed by pancreatic mesenchyme from E9.5 – E11.5 and is required for pancreatic epithelial growth.[31] Fgf10 mutant embryos fail to develop a pancreas because of impaired proliferation of Pdx1+ common pancreatic progenitors.[31]

Meanwhile, an emerging area of research concerns the identity and role of mesenchymal sub-populations in the development of the pancreas,[26] and their mediation of mesenchymal-epithelial interactions. In our previous work, we used single-cell RNA-Sequencing (scRNA-Seq) to reveal a previously unappreciated degree of heterogeneity within the mesenchymal compartment of the developing murine pancreas.[37] In particular, we annotated one subgroup of mesenchymal cells as mesothelial based on the expression of genes known to mark serosal mesothelium in other organs: *Wt1*, Cytokeratin 19 (*Krt19*), and Uroplakin 3B (*Upk3b*).[37–40] The mesothelium plays a well-established role of providing a protective, non-adhesive surface to facilitate smooth intracoelomic movement. This cellular membrane has also been linked to other physiological functions key in serosal homeostasis, such as fluid and particulate transport, immune surveillance, and synthesis of pro-inflammatory extracellular matrix molecules, cytokines, and growth factors.[40–42] Although the mesothelium has also been shown to secrete factors that regulate organ development, such as in the lung[43] and liver,[44] the function of the mesothelium in pancreatic development remains understudied.

In this study, our timecourse scRNA-Seq analyses and *in situ* hybridization (ISH) experiments have revealed the spatial and temporal dynamics of *Fgf9* expression in the developing mouse pancreas. Taken together, our data demonstrate that *Fgf9* expression is principally restricted in early development to the mesenchyme (SMP) and then the mesothelium during early development, then subsequently expressed by both the mesothelium and rare epithelial cells by E12.5 and onwards. The function of FGF9 in pancreatic development was investigated using a *Fgf9* global knockout mouse model. Loss of *Fgf9* led to decreased pancreas and stomach size, as well as asplenia. scRNA-Seq and ISH at E14.5 revealed that global loss of *Fgf9* results in altered transcriptional pathways within the pancreas, specifically dramatic reduction of *Barx1* expression in the pancreatic mesenchyme. Computational analysis of cell-cell interactions predicted that FGF9-FGFR1 acts as the major ligand-receptor pair contributing to Fgf9 signaling pathway activity in the developing pancreas. By applying scRNA-Seq and ISH to human fetal pancreatic tissues, we identified conserved expression patterns of Fgf9 and receptors in human fetal pancreas, suggesting that FGF9 expressed by human pancreatic mesenchyme may similarly affect the development of human pancreas.

RESULTS

Expression pattern of Fgf9 and Fgf receptors throughout pancreatic development

To identify paracrine factors that may mediate epithelial-mesenchymal interactions, we probed our previously published scRNA-Seq dataset of developing mouse pancreas[37] for the expression of secreted factors, their receptors, and downstream targets in three pathways known to have roles in pancreatic development: the FGF, Wnt, and BMP pathways.[30,45] Of the many genes examined, *Fgf9* expression was highly enriched in the mesothelium at E12.5, E14.5, and E17.5, with some expression also detected in rare ductal or endocrine cells (Figures 1A, S1A, and S1B). To confirm the findings from the scRNA-Seq data, we performed multiplexed ISH and immunofluorescence (IF) staining of independent samples of embryonic

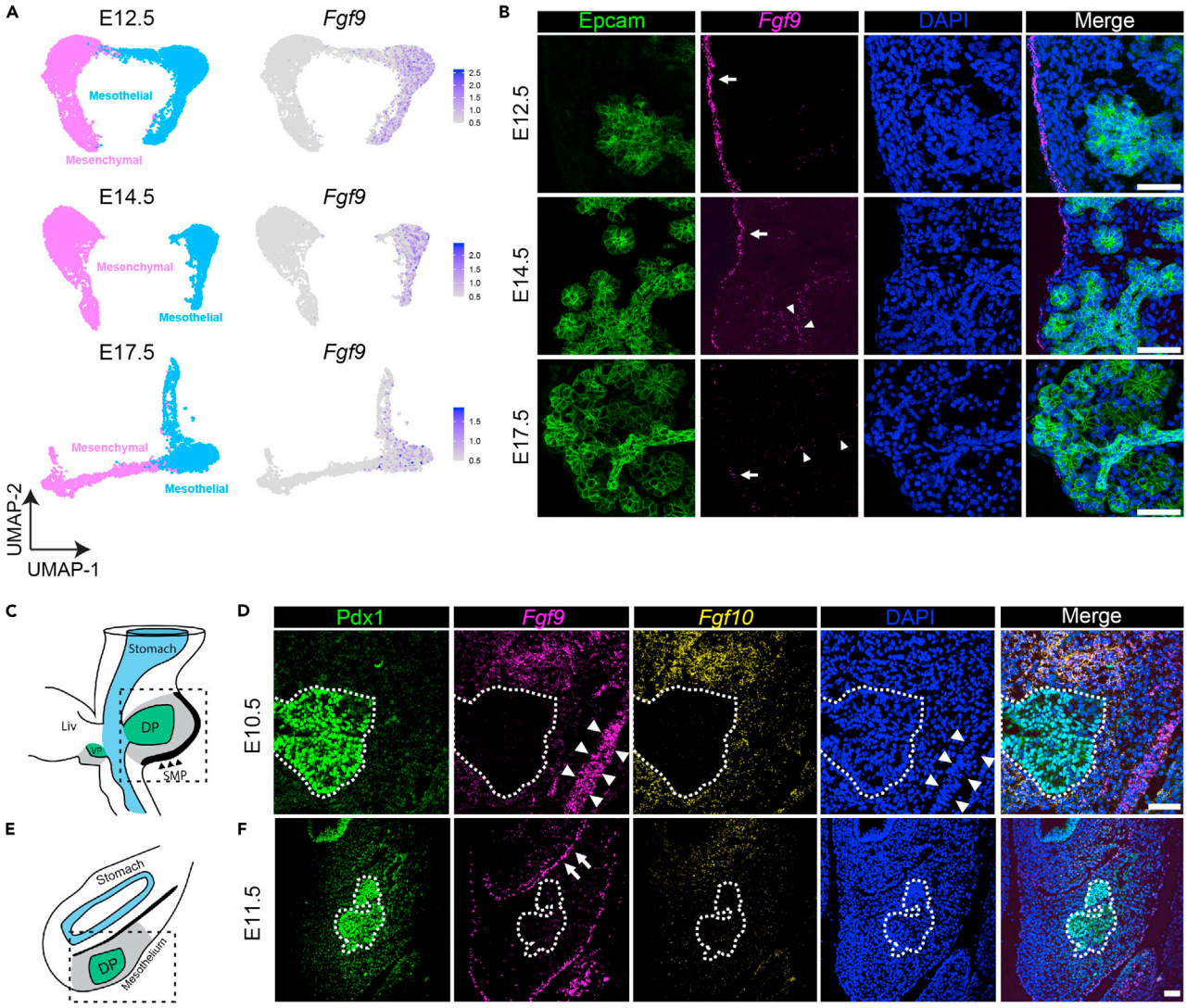

Figure 1. Temporal and spatial dynamics of *Fgf9* expression in the mesenchyme and mesothelium throughout pancreatic development

(A) Left: Uniform manifold approximation and projection (UMAP) plots of single-cell RNA-Sequencing (scRNA-Seq) data from wildtype murine pancreas at embryonic day (E)12.5, E14.5, and E17.5, sub-clustered on Mesenchymal (pink) and Mesothelial (blue) populations only. Cellular populations were annotated based on expression of key marker genes as described in Byrnes et al.[37] Right: Feature plots reveal that *Fgf9* is specifically expressed in the mesothelium at E12.5, E14.5, and E17.5.

(B) Immunofluorescence staining of wildtype mouse E12.5, 14.5, and 17.5 pancreatic tissue. EpCAM protein is shown in green and marks cell membranes of epithelial cells. *Fgf9* transcript is shown in magenta. Arrows point to mesothelial expression, and arrowheads indicate weak ductal expression. DAPI staining of nuclei is shown in blue. Scale bars are 100 μm.

(C) Schematic depicts the orientation of dorsal pancreas (DP) relative to stomach, liver, and splanchnic mesodermal plate (SMP, arrowheads) at E10.5, corresponding to panels in (D).

(D) Immunofluorescence of sagittal sections of pancreas tissue at E10.5. Dashed lines outline the DP. Pdx1 protein marks pancreatic epithelium and is shown in green, *Fgf9* transcript is shown in magenta, *Fgf10* transcript is shown in yellow, and DAPI staining of nuclei is shown in blue. Arrowheads mark *Fgf9* expression in the SMP at E10.5.

(E) Schematic depicts the orientation of the DP relative to the stomach and mesothelium at E11.5, corresponding to panels in (F).

(F) Pdx1 protein staining is shown in green and marks pancreatic epithelium, which is outlined by dashed lines. Arrows mark *Fgf9* expression (magenta) in the mesothelium at E11.5. Scale bars in (D and F) are 50 μm.

mouse pancreatic tissue. We validated that as predicted, from E12.5 to E17.5 *Fgf9* expression was enriched in the *Wt1*-expressing mesothelium at the edge of the tissue (Figures 1B, S1F, and S1H), with low expression in some ductal cells at E14.5 and E17.5 (Figures 1B and S1B).

Fgf10 is expressed by pancreatic mesenchyme from E9.5 to E11.5 and is required for pancreatic epithelial growth.[31] Previously published work did not delineate whether specific sub-populations of mesenchymal cells co-express Fgf9 and Fgf10, so we analyzed the epithelial and mesenchymal expression patterns of *Fgf9* and *Fgf10* in embryonic mouse pancreatic tissue at E10.5 and E11.5. At E10.5, we confirmed that *Fgf9* expression was found primarily in the dorsal SMP, whereas *Fgf10* was primarily restricted to the sub-epithelial mesenchyme (Figures 1C and 1D) and the ventral SMP (data not shown' previously reported by Hecksher-Sorensen et al., 2004). We also found an overlap of *Fgf9* and *Fgf10* transcripts in the mesenchyme between the dorsal pancreatic epithelium and the primordial stomach (Figures 1C and 1D).

By E11.5, *Fgf9* was largely restricted to the mesothelium of the dorsal pancreas (Figures 1E and 1F). In contrast, and consistent with previously published data,[30,31,34] *Fgf10* expression had started to wane by this time. Taken together, our data demonstrate that *Fgf9* expression is principally restricted to the SMP and then the mesothelium during early development, then subsequently expressed by both the mesothelium and rare epithelial cells by E12.5 and onwards. Expression of both *Fgf9* and *Fgf10* is high around E10.5, when there is co-expression in mesenchyme just rostral to the dorsal pancreatic bud. Subsequently, although *Fgf10* expression declines, *Fgf9* persists at E11.5 and onward.

Given the striking pattern of expression of *Fgf9* in developing pancreas tissue, we next asked which cells express the cognate receptors. Prior work attempting to define the expression patterns of Fgf receptors in the developing pancreas has primarily been limited to detection by quantitative real-time polymerase chain reaction (qRT-PCR), which lacks resolution spatially or within cell type.[30,34] FGF9 is capable of signaling through FGFR1c and 2c splice variants, which are typically expressed in mesenchymal tissue, as well as FGFR3b and 3c splice variants, for which tissue-specific regulation of receptor isoform expression is not as strict.[46–48] Thus, we analyzed *Fgfr1-3* expression using scRNA-Seq and multiplexed ISH at multiple timepoints across embryonic development. Our scRNA-Seq data indicated that at E12.5, *Fgfr1* is expressed in mesenchymal cells and in rare epithelial cells, and *Fgfr2* mostly in epithelial cells (Figures S1C and S1D). *Fgfr3* was difficult to detect by scRNA-Seq at this timepoint (Figure S1E). By ISH, we determined that at E10.5, *Fgfr1* was broadly expressed in the dorsal pancreatic mesenchyme, including the mesenchyme directly beneath the SMP and the SMP itself; it was also found in the epithelium (Figure S2A). *Fgfr2* was primarily expressed in the epithelium, and *Fgfr3* was lowly expressed in the mesenchyme and epithelium. At E11.5, *Fgfr1* was again expressed fairly ubiquitously, whereas there was low expression of *Fgf2 and Fgfr3* in Epcam+ epithelial cells (Figure S2A). Both *Fgfr1* and *Fgfr3* were expressed by mesothelial cells. At E12.5, *Fgfr1* was still expressed broadly and *Fgfr2* was primarily restricted to epithelial cells (Figure S2A). *Fgfr3* was expressed in epithelium and mesenchyme, and enriched in the sub-mesothelial mesenchyme. At E14.5, *Fgfr1* was ubiquitously expressed, *Fgfr2* was expressed in epithelial cells (enriched in ducts), and *Fgfr3* was expressed in epithelial cells (enriched in ducts) and lowly expressed in mesenchyme, including mesothelial cells (Figure S2B). By E17.5, *Fgfr1* was expressed in epithelium and mesenchyme at very low levels, *Fgfr2* was expressed at very low levels in ductal cells, and *Fgfr3* was expressed in ductal cells (Figure S2C).

In summary, we have determined that the pancreatic mesenchymally-secreted factor *Fgf9* is expressed by the SMP early in development (E10.5) and then pancreatic mesothelial cells by E12.5. In addition, *Fgf9* is expressed by rare ductal and endocrine cells in late embryonic development. We have also characterized the cell type-specific expression of the various Fgf receptors throughout pancreatic development.

Loss of Fgf9 leads to asplenia and abnormal pancreatic and gastric development

To ascertain the function of Fgf9 in pancreatic development, we utilized a mouse line with a LacZ allele knocked into the *Fgf9* locus, which leads to a functional knockout of the *Fgf9* allele.[49] As previously described,[43] embryos lacking a functional *Fgf9* gene (hereinafter referred to as *Fgf9* null) were smaller overall than their homozygous wildtype (WT) and heterozygous littermates (hereinafter collectively referred to as control) (Figure 2A), and *Fgf9* null mice did not survive postnatally because of hypoplastic lungs leading to respiratory failure. We found that as with the lung phenotype, pancreata of *Fgf9* null mice were also hypoplastic compared to those of their control littermates (Figures 2B–2D). The average weight of *Fgf9* null embryos at E17.5 was 80% that of control littermates ($p < 0.0001$; Figure 2E), yet the ratio of pancreas to whole body weight of *Fgf9* null embryos was only 51% of the controls (0.801% versus 1.576%; $p = 0.0323$; Figure 2F). Thus, the extent of pancreatic hypoplasia was not fully accounted for by the smaller overall size of mutant embryos. At E17.5, *Fgf9* null mice also displayed asplenia, and decreased size of the

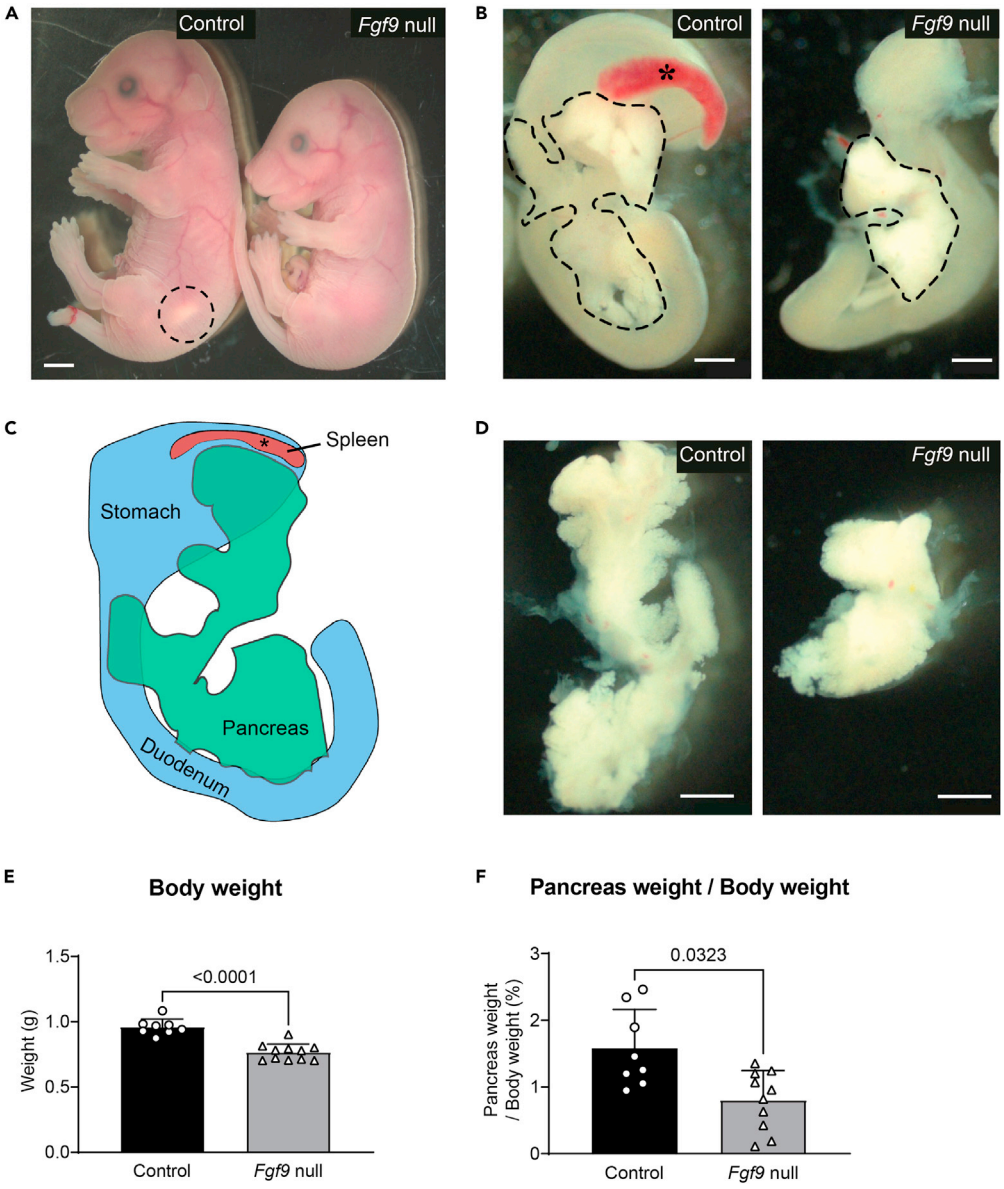

Figure 2. Abnormal pancreatic, splenic, and gastric development in *Fgf9* null mice

(A) At E17.5, *Fgf9* null embryos are smaller overall than control littermates. Dashed circle outlines the visible pancreas in the control embryo. Scale bars are 2 mm.

(B) Representative control and *Fgf9* null pancreata at E17.5 are shown *in situ* and outlined with dashed lines. Asterisk denotes the spleen. In *Fgf9* null embryos, the spleen is entirely absent, while the pancreas and stomach are both decreased in size. Scale bars are 3 mm.

(C) Cartoon depicting normal anatomy of the region of the E17.5 gut tube containing the pancreas.

(D) Gross dissections of control and *Fgf9* null pancreata further reveal significant reduction in the size of the pancreas in the mutant. Scale bars are 3 mm.

(E and F) *Fgf9* null embryos at E17.5 display significantly decreased body weight (E) and pancreatic weight/body weight ratio (F) compared to littermate controls. Each individual embryo is represented as a single data point. Error bars were calculated using standard deviation (SD); statistical significance was determined using an unpaired Student's t-test. n = 8 in the control group; n = 11 in the *Fgf9* null group, from four different litters.

stomach, compared to littermate controls (Figure 2B). In contrast, heterozygous $Fgf9^{LacZ/+}$ embryos and gut tube regions were indistinguishable from WT controls (data not shown). To investigate the possibility that the spleen had been specified earlier but by E17.5 had degraded, we next examined control and null

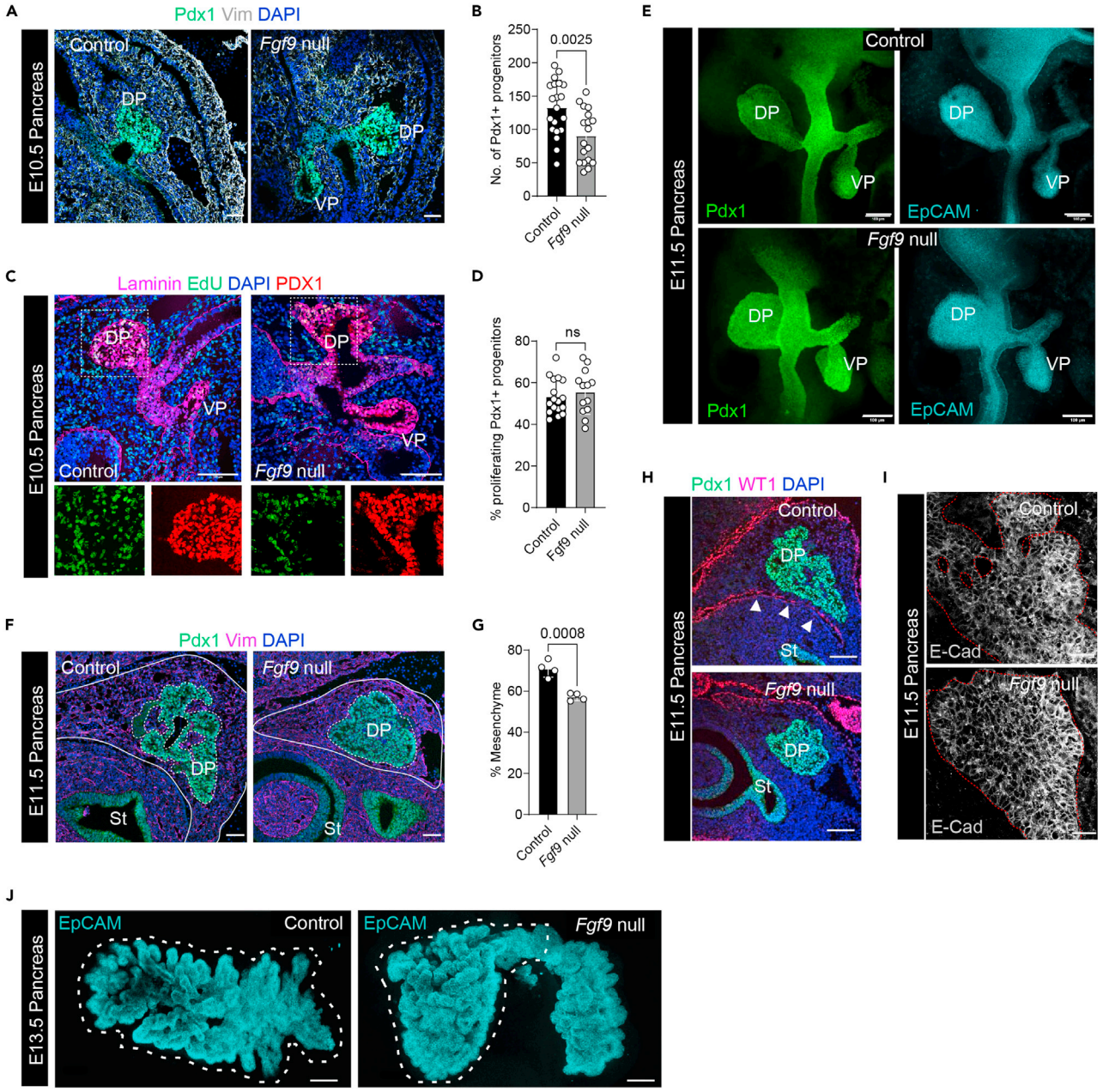

Figure 3. *Fgf9* null pancreata contain reduced numbers of pancreatic progenitors and display defects in epithelial branching morphogenesis and mesothelial development

(A) Immunofluorescence (IF) staining for Pdx1 (marking early pancreatic progenitors at this stage; shown in green) and mesenchymal marker Vimentin (Vim; gray) in E10.5 pancreatic tissue. Nuclei are counterstained with DAPI in blue. Scale bars are 50 μm.

(B) Quantification of Pdx1+ pancreatic progenitor cell number in dorsal pancreata of control (n = 20 sections from 5 embryos) versus *Fgf9* null (n = 18 sections from 5 embryos). Each individual embryo is represented by a single data point. Error bars were calculated using standard deviation (SD); two-tail nested t-test was used to calculate p-value.

(C) E10.5 control and *Fgf9* null pancreatic tissues were profiled for Pdx1 (red), Laminin (magenta), EdU incorporation (green), and DAPI (blue). Scale bars are 100 μm. Single-color images for regions containing dorsal buds are represented below the merged images.

(D) Ratio of proliferating pancreatic progenitor cells in the dorsal pancreas was assessed by calculating the percentage of Pdx1+ cells that were also EdU+ in control (n = 17 sections from 4 embryos) versus *Fgf9* null (n = 13 sections from 4 embryos) dorsal pancreas tissue. Each individual embryo is represented by a single data point. Error bars were calculated using SD; two-tail nested t-test was used to calculate p-value. ns = not significant.

(E) Whole-mount staining of control and *Fgf9* null E11.5 pancreata for Pdx1 (green) and broad epithelial marker EpCAM (Cyan). Both dorsal and ventral pancreas are formed in control and *Fgf9* null embryos. Scale bars are 100 μm.

Figure 3. *Continued*

(F) IF staining for Pdx1 (green) and Vim (magenta) in E11.5 pancreatic tissue. Nuclei are counterstained with DAPI in blue. Dashed lines outline the contour of the Pdx1+ pancreatic epithelium; solid lines outline the contour of the entire pancreatic gland, including epithelium and mesenchyme. Scale bars are25 μm.

(G) Mean mesenchymal area is represented as a percent of total organ area for *Fgf9* null (n = 4) versus control (n = 4) embryonic pancreata at E11.5. Each individual embryo is represented by a single data point. Error bars were calculated using SD; two-tail nested t-test was used to calculate p-value.

(H) IF performed on E11.5 sagittal pancreatic sections reveals loss of mesothelial marker WT1 (indicated by arrowheads, top) in *Fgf9* null tissue. Pancreatic epithelial marker Pdx1 is shown in green, and nuclei are counterstained with DAPI in blue. Scale bars are100 μm.

(I-J) Morphology of the epithelium over developmental time.

(I) IF staining of E11.5 tissue for epithelial marker E-Cadherin (E-Cad) (gray) reveals fewer tubular lumens in *Fgf9* null versus control. Dashed red lines represent the outer layer of the epithelial sheet. Scale bars are 25 μm.

(J) Whole-mount staining of E13.5 control and *Fgf9* null pancreata stained with EpCAM (cyan). Dashed white lines outline the DP. Scale bars are 100 μm. St, stomach. DP, dorsal pancreas; VP, ventral pancreas.

tissues across a timecourse (Figure S3). We found that even at E12.5, *Fgf9* null embryos were completely asplenic (Figure S3). In addition, stomach hypoplasia was visible at least as early as E12.5. Taken together, these data reveal that Fgf9 is required for the proper development of multiple organs of the gastrointestinal tract.

To determine whether the diminished pancreatic size was due to loss of a particular differentiated cell type, we performed IF on E18.5 pancreata from control and *Fgf9* null embryos to detect the major cell lineages (Figures S4A–S4H). In both control and *Fgf9* null pancreata, we identified all of the major lineages of the pancreas, including acinar (Carboxypeptidase A1 (Cpa1)+), ductal and mesothelial (Krt19+), endocrine (Glucagon (Gcg)+ alpha cells, Insulin (Ins)+ beta cells, Somatostatin (Sst)+ delta cells), mesenchymal (Vimentin (Vim)+), nerve (Class III Beta-Tubulin (Tuj1)+), vascular smooth muscle (Smooth muscle actin (SMA)+), and endothelial ($CD31^+$) cells (Figures S4A–S4H). To exclude the possibility that compensation had allowed for recovery of lost cell lineages by late developmental stages, we also verified that these major pancreatic lineages were all present at E12.5, E13.5, and E14.5 in null and control tissues as well (data not shown). Taken together, these results indicate that Fgf9 is not required for the specification of broad lineages in the developing murine pancreas.

Loss of FGF9 results in dynamic shifts in cellular proliferation

We next assessed cell proliferation within the epithelial and mesenchymal compartments of *Fgf9* mutant and control pancreata by calculating rates of incorporation of EdU after exposure *in utero* (Figures S5A–S5F). Mesenchymal proliferation was reduced in *Fgf9* null pancreata relative to controls at E11.5 (30.6% versus 41.2%, p = 0.048), and although there was a trend for reduced epithelial proliferation (35.2% versus 40.9%), it was not statistically significant (p = 0.068) at this timepoint (Figures S5A and S5B). At E12.5, epithelial proliferation was reduced in *Fgf9* null pancreata relative to controls (27.3% versus 38.7%, p = 0.038) but mesenchymal proliferation was unchanged (22.7% versus 22.5%, p = 0.91) (Figures S5C and S5D). By E14.5, there was no difference in proliferation for epithelial (38.9% in null versus 39.6% in control, p = 0.85) or mesenchymal (28.4% in null, 27.6% in control, p = 0.84) cells in *Fgf9* null pancreata relative to controls (Figures S5E and S5F). To assess apoptosis, we stained sections of *Fgf9* null and control pancreatic tissue at E13.5 for cleaved caspase-3. The number of pancreatic cells staining positive for cleaved caspase-3 was negligible in the mesenchyme and epithelium in both conditions (Figure S5G), leading us to conclude that at this timepoint apoptosis is not the primary mechanism underlying pancreatic hypoplasia in *Fgf9* mutants. Thus, although loss of *Fgf9* does not appear to affect cell death in the developing pancreas at later timepoints, it does affect the proliferative capacity of early pancreatic mesenchymal cells and subsequently epithelial cells, likely contributing to the overall reduction in pancreatic size.

Fgf9 null pancreata contain reduced numbers of early pancreatic progenitors and display defects in epithelial structure and mesothelial development

To further understand the cellular mechanisms driving the hypoplastic pancreatic phenotype in *Fgf9* null embryos, we assessed the overall epithelial and mesenchymal morphology at early developmental stages. We validated that both ventral and dorsal buds had formed in control and *Fgf9* null embryos by examining both E10.5 and E11.5 pancreata (Figures 3A and 3E). At E10.5, we quantified the number of epithelial progenitor cells, marked by PDX1 expression at this early developmental stage. We found that the number of early progenitor cells was reduced in the dorsal pancreata of *Fgf9* null compared to control (n = 82 versus 120 per section, respectively; p = 0.0062) (Figures 3A and 3B). That said, we did not observe a reduction in the fraction of epithelial progenitor cells that were proliferating at E10.5, as judged by incorporation of EdU

into PDX1+ cells in the dorsal pancreata of *Fgf9* null (n = 4 embryos, 17 dorsal pancreatic tissue sections) versus control (n = 4 embryos, 13 dorsal pancreatic tissue sections) (Figures 3C and 3D).

We observed an apparent thinning of distal mesenchyme (Figure 3F), indicated by a reduction in the ratio of mesenchymal (VIM+) area to total tissue area (combined area of both VIM+ and epithelial (PDX1+) compartments) in E11.5 *Fgf9* null pancreata relative to controls by 13.5% ($p = 0.0008$; Figure 3G). Because *Fgf9* was predominantly expressed in the mesothelial cells of the wildtype developing pancreas at E11.5, we next sought to assess whether the formation of mesothelial tissue was itself disrupted upon *Fgf9* knockout. In control tissue at E11.5, we observed distinct mesothelial layers expressing *Wt1* that serve as boundaries surrounding both the dorsal pancreas and the stomach, providing clear separation of these organs. In *Fgf9* null embryos, however, the mesothelial layers at the interface of the stomach and dorsal pancreas had failed to form, and the dorsal pancreas was instead adhered to the stomach via intervening mesenchyme (Figure 3H).

Through early gestation, the multi-layered pancreatic epithelium decreases in thickness in a process of de-stratification as branches form.[39] Despite the formation of epithelial branches in both control and *Fgf9* null pancreata, it was apparent this process was delayed in null embryos. Fgf9 derived from mesenchyme or mesothelium may contribute to this de-stratification process, as the difference in epithelial structure observed at E11.5 (Figure 3I), when *Fgf9* is almost exclusively expressed in the mesothelium and sub-mesothelial mesenchyme, becomes less severe by E13.5 (Figure 3J). In summary, although the *Fgf9* null pancreas does contain both ventral and dorsal buds, it contains fewer early epithelial progenitors, likely at least partially explaining the hypoplasia phenotype. In addition, *Fgf9* null pancreatic tissue displays an early defect in epithelial structure, abnormal specification of mesothelial layers, and decreased mesenchymal tissue volume.

Bulk RNA-Sequencing reveals the downregulation of transcription factors controlling mesenchymal development in *Fgf9* null pancreata

To identify the molecular mechanisms underlying the developmental defects observed in *Fgf9* null pancreata, bulk RNA-Seq was performed on dorsal pancreatic tissue from control (including $Fgf9^{+/+}$ and $Fgf9^{LacZ/+}$ pancreata) and null embryos at both E13.5 and E14.5 (Figures S6A–S6D; Table S1). Pathway analysis was performed using ConsensusPathDB on genes differentially expressed between E14.5 control and null pancreata. In the control pancreas, pathways relating to Calcium Signaling, RA biosynthesis, and cAMP signaling were annotated as enriched, while in the null pancreata, pathways relating to extracellular matrix organization and striated muscle contraction were annotated as enriched (Figure S6E). Not surprisingly, given the abnormal morphogenesis of the foregut structures, expression levels of several homeobox genes were dysregulated in the *Fgf9* null pancreata (Figures S6A–S6D). Notably, the expression levels of several transcription factors known to be essential for normal spleen and pancreatic development were downregulated, including T Cell Leukemia Homeobox 1 (*Tlx1*), BARX Homeobox 1 (*Barx1*), NK2 Homeobox 5 (*Nkx2.5*), and *Nkx3.2* (Figures S6A–S6D; Table S1). Tlx1 is normally expressed in the spleno-pancreatic mesenchyme.[50,51] *Tlx1* knockout mice lack a spleen because of failed expansion of spleen primordium; whereas the region of the dorsal mesogastrium where the spleen normally forms remains fused with the stomach, animals do form a pancreas.[50–52] Barx1 is expressed in the SMP at E9.5-E10.5, later in the mesogastrium in which the pancreas and spleen form, and eventually in the mesothelium surrounding both of these organs, and is important for proper positioning and expansion of the spleen.[19,53,54] *Barx1* knockout mice have a markedly hypoplastic spleen that lacks a normal WT1-expressing mesothelial capsule and is abnormally located within the dorsal pancreas.[54] In addition, the dorsal and ventral pancreatic buds do not fuse, which is thought to be because of abnormal rotation of the gut.[54] In our bulk RNA-Seq dataset, *Barx1* showed reduced expression in the *Fgf9* null pancreata at both E13.5 and E14.5 (Figures S6A–S6D, Table S1). Our scRNA-Seq data further revealed that Fgf9 knockout results in the diminished expression of *Barx1* specifically in the mesenchymal populations, a finding that was validated in tissue sections with ISH (Figure 7F).

Nkx2.5 and Nkx3.2 mark the two lineages that make up the majority of the pancreatic mesenchyme (Landsman et al., 2011; Cozzitorto et al. 2020) and were both down-regulated at E13.5 (Table S1). *Nkx2.5* null embryos die around E10, thus insights into pancreatic development using this model are limited. Nevertheless, there is clear *Nkx2.5* expression in the early spleno-pancreatic mesenchyme at E10.5, after which point expression remains in the spleen but is reduced in the pancreas, and becomes

restricted to expression in mesenchyme surrounding the left side of the dorsal pancreas.[26,55,56] Nkx3.2 is also expressed in early splenopancreatic mesenchyme, and Nkx3.2 lineage-traced cells make up the majority of pancreatic mesenchyme.[21,26] Nkx3.2 is an essential transcription factor for proper formation of the SMP and lateralization of the spleen and pancreas.[19,57] Taken together, these data demonstrate that FGF9 functions as a secreted factor that is an essential mediator of gut patterning.

LIM Homeobox 9 (*Lhx9*) expression was also decreased in the *Fgf9* null pancreata at both E13.5 (Figure S6C, Table S1) and E14.5 (Figures S6B and S6D; Table S1). *Lhx9* is a member of the LIM-homeodomain gene family, and is necessary for the proper development of many organs, including gonads, limbs, heart, and the nervous system.[58–62] Initiation and maintenance of *Lhx9* expression is dependent on Fgf signaling in limbs and the brain,[63,64] and based on our results, in the pancreas it appears to also be dependent on *Fgf9*. The expression of the transcription factor Paired-related homeobox 1 (*Prrx1*) was reduced in the *Fgf9* null pancreata (Figures S6C and S6D; Table S1). Prrx1 has been previously characterized as a marker of a mesenchymal subpopulation in mouse dermis,[65] and as an important transcription factor regulating the maturation of cranial neural crest to a more mature mesenchymal state.[66]

There were several genes up-regulated in *Fgf9* null pancreata at E13.5 (Figures S6A and S6C; Table S1) and E14.5 (Figures S6B and S6D; Table S1). For example, Early growth response protein 1 (*Egr1*), a gene reported to regulate transcription of *Insulin*, was up-regulated at both timepoints. Insulinoma-associated 2 (*Insm2*) was upregulated at E13.5 (Figures S6A and S6C; Table S1), and targeted deletion of *Insm2* in mouse pancreas leads to reduced insulin secretion.[67,68] Onecut2 (*OC-2*) was another up-regulated transcription factor at E14.5 (Figure S6D; Table S1). OC-2 is a paralog of HNF-6 and has been previously shown to be important in expansion of the dorsal pancreas and the number of Neurog3+ cells, potentially through direct binding of the Neurog3 promoter.[69]

Single-cell RNA-Seq reveals that all major cell lineages are generated in *Fgf9* null embryos

Results of the bulk RNA-Seq experiments were informative regarding alterations in global gene expression profiles of control versus *Fgf9* null embryonic pancreata, particularly with respect to the expression of genes such as transcription factors that may be relatively lowly expressed. Still, this bulk technique does not provide information about relative changes in cell populations between the two conditions. To gain single-cell resolution with respect to gene expression and to determine whether shifts in cell populations occurred in the pancreas as a result of *Fgf9* loss, we next performed scRNA-Seq on control and null pancreatic tissue at E14.5. E14.5 represents a dynamic timepoint in development at which the processes of proliferation, cell fate determination, and maturation are occurring simultaneously in the pancreas, and it corresponds to the timepoint of greatest focus in our previous scRNA-Seq study.[37]

Eight control and six *Fgf9* null pancreata from three litters were pooled separately and subjected to the 10x Genomics Chromium Single Cell 3′ v3.1 sequencing platform. After computational filtering, we obtained 12,467 quality cells in the control group and 7,249 in the *Fgf9* null group, and merged them into a single integrated dataset for clustering and annotation of cell populations based on expression of key marker genes (Figures 4A and 4B). By assessing the contribution of cells from both control and *Fgf9* null pancreata to the merged dataset, we determined that both genotypes contained all of the main pancreatic cell lineages, including ductal (*Sox9+*), acinar (*Cpa1+*), endocrine progenitor (*Neurog3+*), hormone-producing *(Chromogranin A (Chga)+*), mesothelial (*Wt1+*), mesenchymal (*Col1a1+*), endothelial (*Pecam1+*), immune (*Rac2+*), and proliferating (*Top2a+*) cells (Figures 4A and 4B; Table S2), indicating that deletion of *Fgf9* in the pancreas did not prevent fate specification of any broad cell type. This observation further confirmed our observations previously made through IF staining *in vivo* (Figure S4).

Although the *Fgf9* null tissue contained all of the same broad pancreatic lineages as the control tissue, some lineages were computationally predicted to be shifted in relative abundance. Specifically, compared to control pancreata, the proportions of acinar and hormone-expressing endocrine populations (alpha, beta, delta, and epsilon) were computationally predicted to be increased in the null pancreata, whereas the relative proportion of mesenchymal populations was predicted to be decreased (Figure 4C). The reduced abundance of mesenchyme (representing 17.3% versus 9.7% of total cells in control versus *Fgf9* null, respectively) is consistent with the mesenchymal developmental defect observed in the null tissues (Figures 3F and 3G).

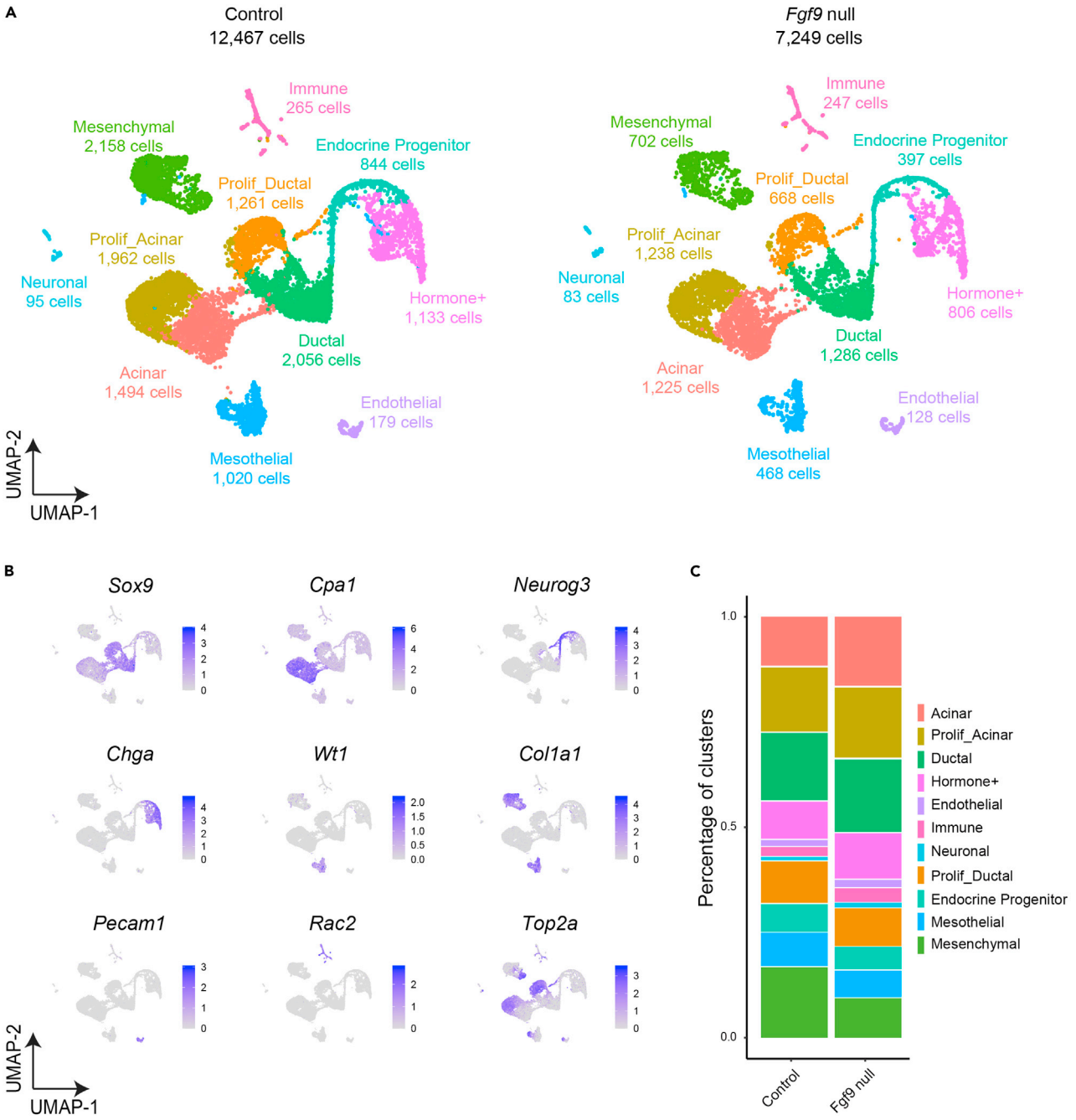

Figure 4. Single-cell RNA-Sequencing data reveal that all major pancreatic cell lineages are generated despite loss of *Fgf9*

(A) Split UMAP plot reveals the broad cellular groups present in E14.5 control (left) and *Fgf9* null (right) mouse pancreas detected by single-cell RNA-Sequencing (scRNA-Seq), as well as the relative contribution of control and null samples to each cell population. Data are derived from eight pooled control pancreata, and six pooled *Fgf9* null pancreata, from three litters.

(B) Feature plots show expression of marker genes in the merged control and null scRNA-Seq dataset. Expression of *Sox9, Cpa1, Neurog3, Chga, Wt1, Col1a1, Pecam1, Rac2,* and *Top2a* marks ductal, acinar, endocrine progenitor, differentiated endocrine, mesothelial, mesenchymal, endothelial, immune, and proliferating cells, respectively.

(C) Analysis of cellular composition between the scRNA-Seq datasets suggests a potential increase in the relative proportion of acinar cells and in differentiated hormone+ endocrine cells, as well as a potential decrease in mesenchymal lineages, in *Fgf9* null pancreata compared to control tissue.

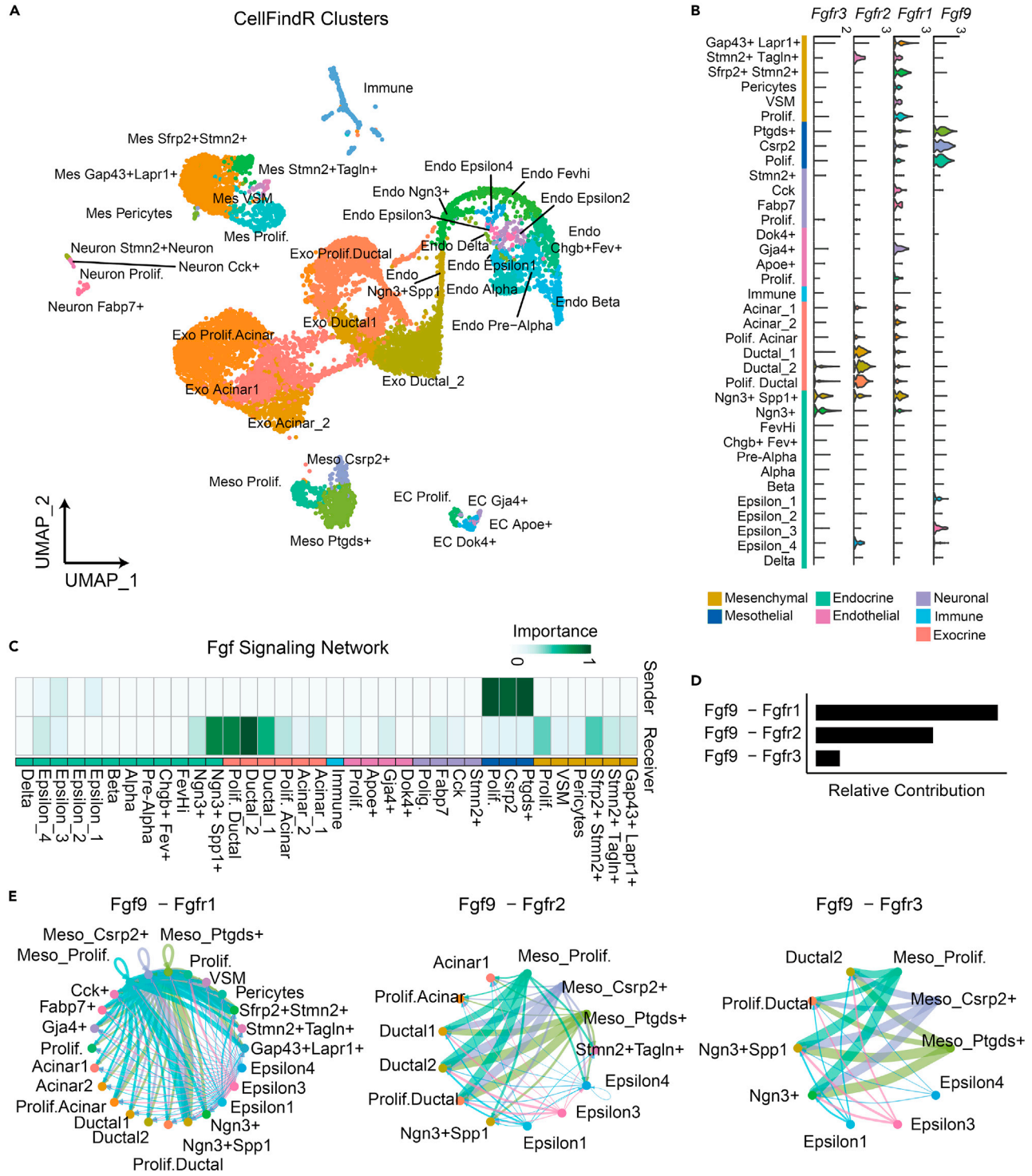

Figure 5. Mesothelial cells are predicted to communicate with multiple other cell types through Fgf9 signaling

(A) Higher resolution clustering of scRNA-Seq data reveals the full panoply of cell populations present in wildtype E14.5 mouse pancreatic tissue. Merged UMAP of control and *Fgf9* null tissue reveals further sub-clustering of cellular populations present in Figure 4A, as annotated by the CellFindR algorithm.

(B) Violin plots show the expression levels of *Fgf9*, along with Fgf9 receptors *Fgfr1*, *Fgfr2*, and *Fgfr3*, in each of the cellular populations identified by CellFindR in (A).

(C) Heatmap designates whether each subpopulation is predicted by CellChat analysis to act as a "Sender" or "Receiver" of Fgf signaling in the E14.5 control dataset.

Figure 5. *Continued*

(D) CellChat analysis predicts the relative contribution of each FGF9-FGFR signaling pair to overall Fgf9 signaling active within the pancreas at E14.5.
(E) Circle plots show the cell type-specific signaling predicted for each FGF9-FGFR ligand-receptor pair, across all populations in which signaling is predicted to occur for that pair. Line thickness is proportional to signaling strength, and line colors represent which population is annotated as the "Sender" of FGF9. Mes, mesenchymal; Meso, mesothelial; EC, endothelial cell; Endo, endocrine; Exo, exocrine; Prolif., proliferating.

Mesothelial cells are predicted to communicate through Fgf9 signaling with multiple other cell types

FGF9 activates downstream signaling by binding to FGFR1, FGFR2, and FGFR3 receptors on the cell surface.[47] To further investigate the cell types that produce Fgf9 and respond to Fgf9 signal by expressing cognate receptors, we decided to explore the cellular heterogeneity within the pancreatic tissue. We applied the clustering algorithm CellFindR, which iteratively increases Louvain clustering resolution based on the condition that each cluster expresses a minimum of 10 genes with greater than two-fold expression in comparison to all other clusters.[70,71] Within E14.5 control pancreas, CellFindR identified a total of 36 distinct cell sub-clusters, including six mesenchymal, three mesothelial, four endothelial, four neuronal, six exocrine, 12 endocrine, and one immune sub-cluster (Figure 5A). Each of these sub-populations identified by CellFindR was annotated according to genes differentially expressed in one cluster over the rest (Table S3).

Next, we examined the expression of *Fgf9* and *Fgfrs* (*Fgfr1-3*) in each subpopulation identified by CellFindR (Figure 5B). At E14.5, *Fgfr1* was broadly expressed in mesenchymal, mesothelial, endothelial, neuronal, acinar, and ductal cells, with enrichment in Neurog3+ and Neurog3+Spp1+ endocrine progenitors (EPs). In contrast, *Fgfr2* was restricted to the Stmn2+Tagln+ mesenchymal cluster, ductal cells, and Neurog3+Spp1+ early EPs. *Fgfr3* was found in Neurog3+ and Neurog3+Spp1+ early EPs and (lowly) in ductal cells. *Fgf9* was highly expressed by the mesothelial cell populations (Meso Ptgds+; Meso Csrp2+; Meso Prolif.) at E14.5 (Figure 5B), corroborating our ISH staining (Figures 1B and S1G).

We next applied the CellChat algorithm[72] to our scRNA-Seq dataset to interpret the aggregated Fgf-Fgfr signaling network among E14.5 control pancreatic cell populations. CellChat placed mesothelial cells (Meso Ptgds+; Meso Csrp2+; Meso Prolif.) as the "Senders" of FGF ligands, and ductal cells, Neurog3+Spp1+ and Neurog3+ EPs, and Sfrp2+Stmn2+ mesenchymal cells as the main "Receivers" of FGF ligands (Figure 5C). Of the FGF9-FGFR interaction pairs assessed by CellChat, the FGF9-FGFR1 ligand-receptor pair was predicted to contribute most significantly to the total Fgf signaling network in the dataset (Figure 5D). The Senders and Receivers of each signaling pair were further illustrated by CellChat Circle Plots (Figure 5E). Taken together, CellChat analysis suggested that at E14.5 FGF9 is secreted by the pancreatic mesothelial population and signals to a range of populations through FGFR1, and to ductal and EP cells through FGFR3. The computational predictions generated here warrant validation with future mouse genetic studies.

Loss of Fgf9 does not alter specification of pancreatic endocrine cell fate

Given the observation that the receptors *Fgfr1*, *Fgfr2*, and *Fgfr3* are expressed in the progenitor populations of the E14.5 pancreatic endocrine compartment (Figures 5B–5E), we hypothesized that FGF9-FGFR signaling may play a role in pancreatic endocrine development. We subsetted the endocrine compartment from the integrated dataset (control and null) and found that CellFindR identified 12 sub-clusters of endocrine cells (Figure 6A). We annotated each population according to the expression of marker genes, including hormones Gcg to mark alpha cells, Ins to mark beta cells, Sst to mark delta cells, and ghrelin (Ghr) to mark epsilon cells, as well as the EP marker *Neurog3* (*Ngn3*) and the transcription factor *Fev*, which we previously discovered marks an EP population downstream of Neurog3 expression and upstream of hormone acquisition.[37] This led to the assignment of three EP clusters ($Ngn3^{+}Spp1^{+}$; $Ngn3^{+}$; Fev^{Hi}) and seven Chga-expressing differentiated endocrine cell clusters (Chgb+Fev+; Pre-Alpha; Alpha; Beta; Delta, and Epsilon clusters 1 through 4 (Figures 6A and S7A). Differentially expressed genes between control and null tissues were calculated for the 12 sub-clusters annotated by CellFindR within the endocrine compartment (Table S4).

Computational analysis revealed the expression patterns of Fgf receptors in the subsetted endocrine dataset. *Fgfr1* and *Fgfr3* receptors were enriched in Ngn3+ and Ngn3+Spp1+ EPs, whereas *Fgfr2* was more restricted specifically to the Ngn3+Spp1+ EPs (Figure 6B). We further validated the expression patterns

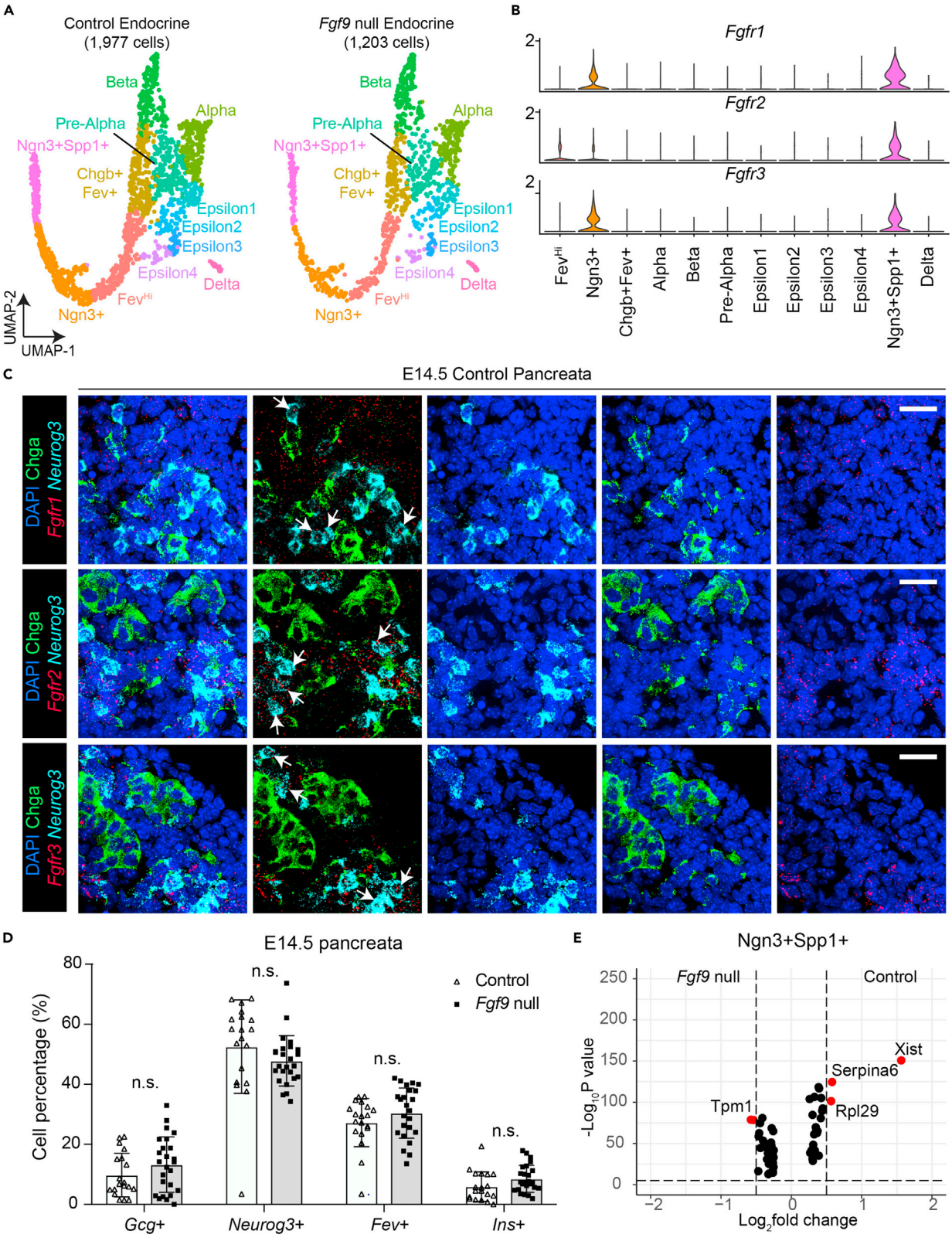
A
Control Endocrine
(1,977 cells)
Fgf9 null Endocrine
(1,203 cells)
Beta
Alpha
Pre-Alpha
Ngn3+Spp1+
Chgb+
Fev+
Epsilon1
Epsilon2
Epsilon3
Epsilon4
Delta
Fev^Hi
Ngn3+
UMAP-2
UMAP-1
B
Fgfr1
Fgfr2
Fgfr3
Fev^Hi
Ngn3+
Chgb+Fev+
Alpha
Beta
Pre-Alpha
Epsilon1
Epsilon2
Epsilon3
Epsilon4
Ngn3+Spp1+
Delta
C
E14.5 Control Pancreata
DAPI Chga Fgfr1 Neurog3
DAPI Chga Fgfr2 Neurog3
DAPI Chga Fgfr3 Neurog3
D
E14.5 pancreata
Cell percentage (%)
Control
Fgf9 null
n.s.
Gcg+
Neurog3+
Fev+
Ins+
E
Ngn3+Spp1+
Fgf9 null
Control
Xist
Serpina6
Rpl29
Tpm1
-Log10 P value
Log2fold change

Figure 6. Loss of *Fgf9* does not alter the relative cellular proportions of endocrine progenitors or the major hormone-producing endocrine lineages in the pancreas

(A) Split UMAP depicts the cell clusters present within the sub-clustered endocrine compartment from the E14.5 merged control and *Fgf9* null dataset, as well as the contribution to the merged dataset from control (left) and *Fgf9* null (right) tissue.

(B) Stacked violin plots show the expression of Fgf receptors in the merged (*Fgf9* null and control) endocrine dataset.

(C) Multiplexed *in situ* hybridization for *Neurog3* (cyan) and *Fgfr1/Fgfr2/Fgfr3* transcripts (red) and immunofluorescence for Chga (green) in E14.5 control pancreatic tissue. Nuclei were counterstained with DAPI (blue). Arrows represent Neurog3+Fgfr+ double-positive cells. Scale bars are 25 μm.

(D) Bar graph showing the percent of all counted cells that were Gcg+, Neurog3+, Fev+, or Ins+ cells in control pancreata (n = 3 biological samples; 19 ROIs; 1,579 cells counted) or *Fgf9* null pancreata (n = 2 biological samples; 24 ROIs; 2,711 cells counted). Quantification was performed on images generated by *in situ* hybridization/immunofluorescence; representative images are shown in Figure S7C. n.s. not significant. Error bars were calculated using standard deviation (SD); unpaired t-test was used to calculate p-values.

(E) Volcano plot depicting the differentially expressed genes in the Ngn3+Spp1+ population in control versus *Fgf9* null tissue.

of *Fgfr1-3* using multiplexed ISH/IF staining to detect Fgf receptor expression in differentiated endocrine (Chga+) cells and in EP cells (*Neurog3+*). In E14.5 control pancreatic tissue *Fgfr1* was expressed broadly across cellular populations, except in the mature endocrine populations (Figure 6C), which was consistent with our scRNA-Seq analysis (Figure 5B). *Fgfr2* and *Fgfr3* were enriched in Neurog3+Chga- cells (Figure 6C).

To elucidate whether Fgf9-Fgfr signaling indeed plays a role in endocrine cell fate specification, we evaluated the relative proportion of each endocrine cell type from the null and the control sample of the endocrine datasets. Consistent with IF data in Figure S4, the null pancreata contained all the same endocrine populations present in the control tissue. The relative proportions of these populations varied, however, with a predicted decrease in the total proportion of EP populations and a predicted increase in the proportion of alpha and beta populations in the *Fgf9* null pancreata (Figure S7B). We performed multiplexed ISH staining to detect the *Ngn3+*, *Fev+*, *Ins+*, or *Gcg+* cells in independent biological samples of E14.5 control (n = 3; 1,579 cells counted) and null (n = 2; 2,711 cells counted) pancreas tissue (Figure S7C). In contrast to the predictions generated from the scRNA-Seq data, the ratios of EP cell populations (*Ngn3+* or *Fev+*) or differentiated hormone populations (*Gcg+* or *Ins+*) at E14.5 were not significantly altered between control and null pancreata (Figure 6D). In addition to measuring changes in relative abundance of each endocrine subpopulation, we also assessed whether there were transcriptional changes within each endocrine subpopulation in the control versus null tissue. We found very few genes differentially expressed between control and null tissue, for any of the endocrine sub-populations present (Table S4). Representative data are shown for the Ngn3+Spp1+ population, where only a handful of genes show differential expression (Figure 6E). Together, our findings suggest that the hypoplastic pancreatic phenotype in *Fgf9* null embryos is likely not reflective of broad alterations in cell specification or in transcriptional programs within the pancreatic endocrine lineage at E14.5.

Loss of Fgf9 does not result in loss of pancreatic mesenchymal populations

The CellChat analysis described above had predicted that at E14.5, all pancreatic mesenchymal cell populations receive FGF9 signal through FGFR1 (Figure 5E). Based on this analysis, we sought to evaluate whether knockout of *Fgf9* affects mesenchymal fate specification. We subsetted the mesenchymal compartment from the E14.5 integrated dataset (control and null), and re-clustered with CellFindR, which identified nine clusters of mesenchymal cells, including mesothelial cells (Figure 7A). The largest mesenchymal cluster, Gap43+Lpar1+, was annotated according to the enriched expression of growth associated protein 43 (*Gap43)* and lysophosphatidic acid receptor 1 (*Lpar1)* genes. The second largest cluster, annotated as Sfrp2+Stmn2+, highly expressed chemokine C-X-C motif chemokine ligand 12 (*Cxcl12*) and Wnt antagonist secreted frizzled related protein 2 (*Sfrp2)*. The Sfrp2+Tagln+ cluster was enriched in expression of *Sfrp2* and Transgelin (*Tagln*); the VSM cells highly expressed smooth muscle α-2 actin (*Acta2*) and *Tagln*; Pericytes expressed the characteristic gene Platelet-derived growth factor receptor beta (*Pdgfrb*); and the proliferating clusters (Mes_Prolif.) highly expressed proliferation marker *Mki67* and Topoisomerase IIα (*Top2a*) (Figures 7A, S8A, and S8B). The three mesothelial populations identified by CellFindR algorithm included a prostaglandin D2 synthase (*Ptgds*)-expressing population, and a Cysteine and Glycine Rich Protein 2 (*Csrp2*)-expressing population, as well as a proliferating (Meso_Prolif.) population.

We compared the mesenchymal cell populations from control and null pancreata and found no evidence that mesenchymal lineages were either lost or newly appeared on *Fgf9* knockout, suggesting that Fgf9 is not required for mesenchymal cell fate specification (Figures 7A and 7B). That said, in null pancreata the percentage of Gap43+Lapr1+ mesenchymal cells appeared to decrease, whereas the percentage of

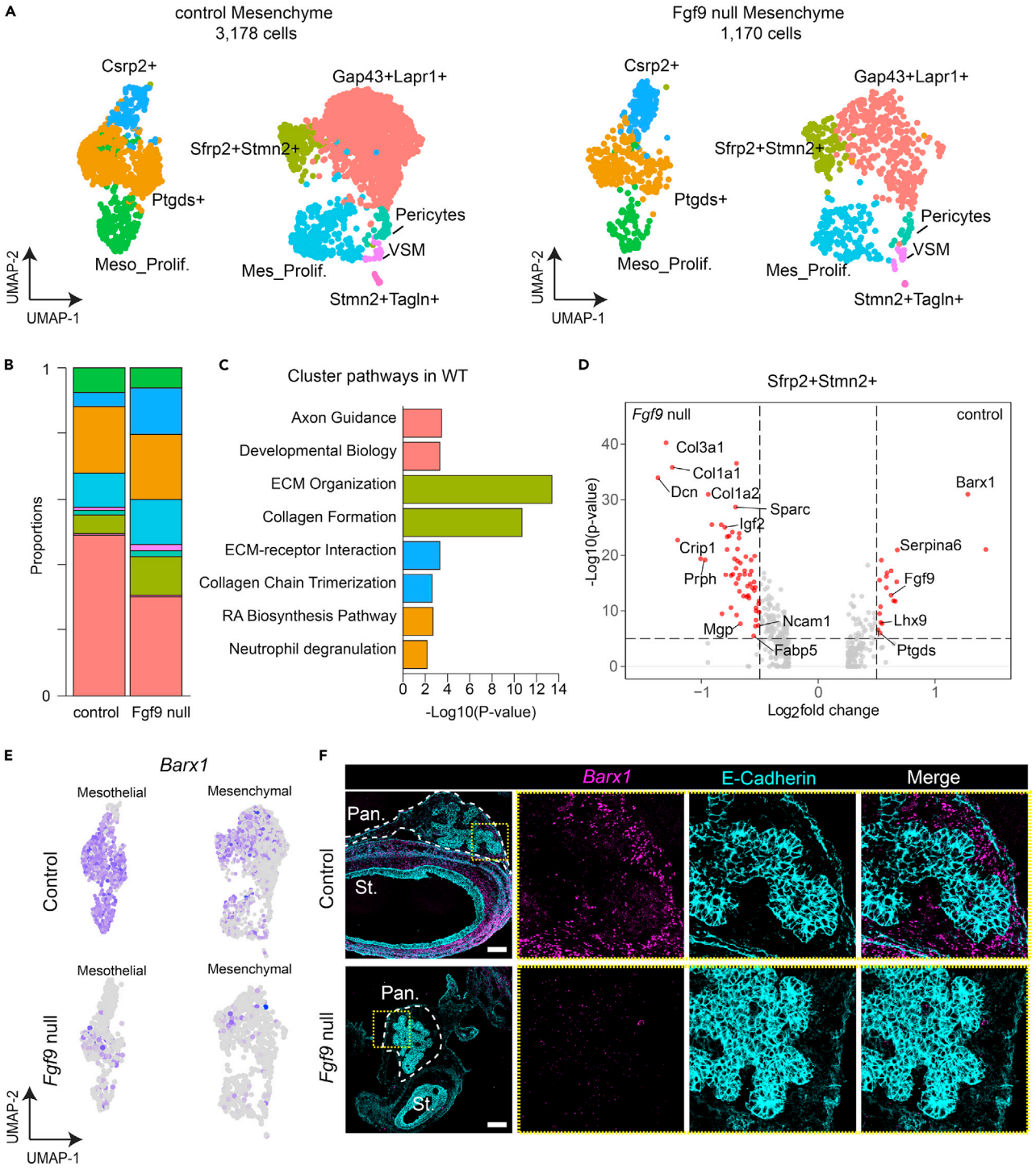

Figure 7. Mesenchymal cell specification is not affected by loss of *Fgf9*

(A) Split UMAP depicts the cellular subtypes present within the sub-clustered mesenchymal compartment of E14.5 control (left) and *Fgf9* null (right) mouse pancreas. Sub-populations are annotated based on expression of genes as shown in Figure S8.

(B) Quantification of data in (A) suggests changes in cellular proportions within the mesenchyme of *Fgf9* null pancreas, including a possible decrease in the mesenchymal Gap43+Lpar1+ subpopulation, and a possible increase in the mesenchymal Sfrp2+Stmn2+ subpopulation and in the mesothelial Csrp2+ subpopulation, relative to control pancreas.

(C) Pathway analysis reveals signaling pathways that are enriched within selected sub-populations. Selected pathways are shown.

Figure 7. *Continued*

(D) Enhanced volcano plot depicting genes differentially expressed between control and *Fgf9 null* pancreas, within the Sfrp2+Stmn2+ mesenchymal population.

(E) Feature plots reveal that *Barx1* expression is significantly decreased in *Fgf9* null mesenchyme and mesothelium compared to control at E14.5. Population annotation is as shown in (A).

(F) Multiplexed *in situ* hybridization/immunofluorescence staining validates that *Barx1* (magenta) is strongly expressed in control pancreatic and stomach mesenchyme at E14.5. In contrast, no appreciable *Barx1* is detected in pancreatic or stomach mesenchyme in *Fgf9* null embryos. E-cadherin (cyan) marks epithelial cells. Pan., pancreas; St., stomach. Dashed lines outline the pancreas. Inserts show enlarged representative areas, as outlined by dashed yellow squares. Scale bars are 100 μm.

Sfrp2+Stmn2+ mesenchymal cells and of Csrp2+ mesothelial cells appeared to increase (Figure 7B). These two increased populations may be involved in extracellular matrix (ECM) regulation in the mesenchyme, as the signaling pathways enriched in the Sfrp2+Stmn2+ subpopulation included ECM organization and collagen formation, whereas the enriched signaling pathways enriched in the Csrp2+ mesothelial population included ECM-receptor interaction and collagen chain trimerization (Figure 7C). We next calculated the changes in gene expression within each mesenchymal cell population between control versus null tissue (Table S5). Control Sfrp2+Stmn2+ cluster showed higher expressed levels of *Barx1*, *Fgf9*, and *Lhx9*, whereas Sfrp2+Stmn2+ cells in *Fgf9* null tissue were enriched in ECM genes such as *Col3a1*, *Col1a1*, *Col1a2, Mgp,* and *Dcn* (Table S5; Figure 7D). The largest mesenchymal population, the Gap43+ Lapr1+ cluster, also showed increased expression of Actin and ECM genes, such as *Acta2*, *Col14a1*, *Fn1*, and *Fbn1* in the null versus control (Table S5). Consistent with our observations from bulk RNA-Seq (Figure S6), the expression of *Barx1* was lower in all mesothelium and mesenchyme clusters from null embryos in the scRNA-Seq dataset as well (Table S5; Figure 7E). We further validated these observations with multiplexed ISH/IF staining for *Barx1* and the epithelial marker E-cadherin on E14.5 embryonic sagittal sections. In control pancreata, we detected restricted expression of *Barx1* in the mesenchyme and mesothelium region of the stomach and pancreas, but not in the E-cadherin+ epithelium (Figure 7F). In E14.5 null pancreata, *Barx1* signal was undetectable in the mesenchyme of pancreas by ISH, corroborating our observations via bulk RNA-Seq and scRNA-Seq (Figure 7F). We conclude that *Fgf9* is required for the normal composition of mesenchymal populations and ECM-associated gene expression. *Fgf9* regulates the expression of *Barx1* by pancreatic and gastric mesenchyme, and the molecular mechanisms underlying Barx1 function in pancreatic development warrants further investigation.

FGF9 signaling in the developing human pancreas

Based on our murine studies described here, we next sought to elucidate whether there was conservation of mouse *Fgf9* and *Fgfr* expression in the developing human pancreas. In other work from our laboratory, we have generated a scRNA-Seq atlas of eight biological samples of human fetal pancreas ranging from 8 to 20 weeks post conception (wpc), containing transcriptomic information from a total of 114,837 cells.[73] We evaluated the expression profiles of *FGF9* and all of the *FGF* receptors in this integrated dataset containing endothelial, mesenchymal, exocrine, endocrine, immune, neuronal, and proliferating lineages (Figure S9A). We found that *FGFR1* was enriched in endothelial, mesenchymal, exocrine, and proliferating cells, with mesenchymal cells showing the highest levels (Figures S9B and S9C). *FGFR2* and *3* showed relatively low expression across the dataset, mostly within exocrine cells. Lastly, *FGFR4* showed strong expression in exocrine and proliferating (likely also exocrine) cells (Figures S9B and S9C).

At this level of resolution by clustering on broad groups, it was initially challenging to detect *FGF9* expression in the overall merged dataset (Figures S9B and S9C). Given our findings that in murine pancreas *Fgf9* is expressed in the mesenchyme and mesothelium, we focused on the expression patterns of *FGF9* and *FGFRs* in the mesenchymal compartment of the developing human fetal pancreas. Obtaining data on mesothelial cells from human samples can be challenging as they are a rare cell type and can often be lost when this outer layer is damaged during tissue dissection, but fortunately we were able to obtain a small number (265 out of 53,941 mesenchymal cells) of mesothelial cells in this human dataset (Figure 8A).[73] Similar to the mouse pancreas, in the annotated human fetal mesenchymal dataset we found that *FGF9* was indeed expressed by mesothelial cells, which were annotated according to expression of mesothelial markers Keratin 19 (*KRT19*), Mesothelin (*MSLN*), and *WT1* (Figures 8A and 8B). *FGFR1* was expressed fairly broadly across all mesenchymal clusters, whereas *FGFR2-4* were barely detected in any of the mesenchymal sub-clusters (Figure 8B). Given the relatively low number of mesothelial cells captured by scRNA-Seq, we used multiplexed ISH/IF staining to validate the expression of FGF9 and receptors in an independent biological sample of human fetal pancreas at 9 wpc (Figures 8C–8G and S9D). To highlight the

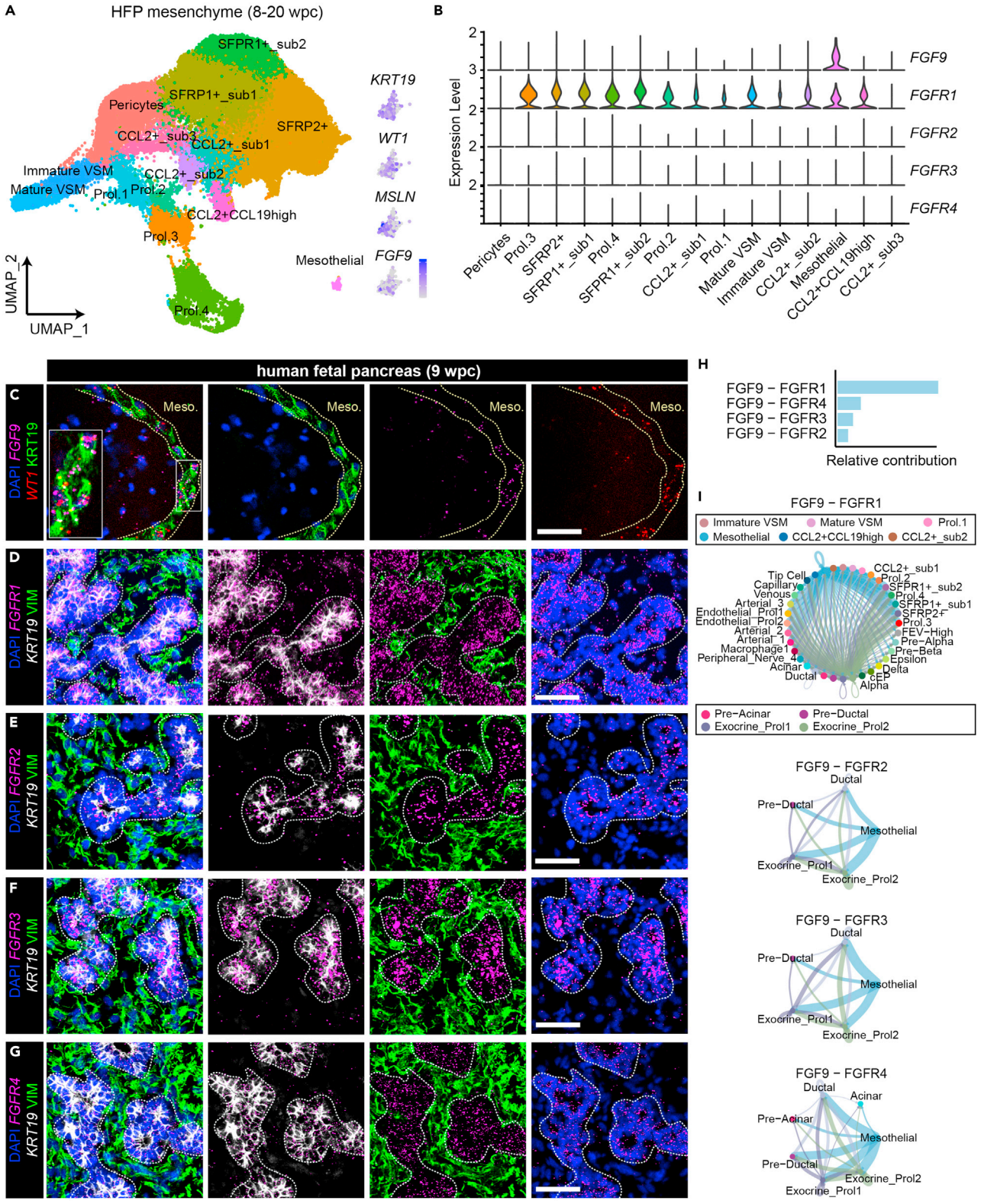
A
HFP mesenchyme (8-20 wpc)
SFPR1+_sub2
SFRP1+_sub1
Pericytes
SFRP2+
CCL2+_sub3
CCL2+_sub1
Immature VSM
CCL2+_sub2
Mature VSM
Prol.1
Prol.2
CCL2+CCL19high
Prol.3
Prol.4
UMAP_2
UMAP_1
KRT19
WT1
MSLN
Mesothelial
FGF9
B
Expression Level
FGF9
FGFR1
FGFR2
FGFR3
FGFR4
Pericytes
Prol.3
SFRP2+
SFRP1+_sub1
Prol.4
SFRP1+_sub2
Prol.2
CCL2+_sub1
Prol.1
Mature VSM
Immature VSM
CCL2+_sub2
Mesothelial
CCL2+CCL19high
CCL2+_sub3
human fetal pancreas (9 wpc)
C
DAPI FGF9 WT1 KRT19
Meso.
D
DAPI FGFR1 KRT19 VIM
E
DAPI FGFR2 KRT19 VIM
F
DAPI FGFR3 KRT19 VIM
G
DAPI FGFR4 KRT19 VIM
H
FGF9 – FGFR1
FGF9 – FGFR4
FGF9 – FGFR3
FGF9 – FGFR2
Relative contribution
I
FGF9 – FGFR1
Immature VSM
Mature VSM
Prol.1
Mesothelial
CCL2+CCL19high
CCL2+_sub2
Tip Cell
Capillary
Venous
Arterial_3
Endothelial_Prol1
Endothelial_Prol2
Arterial_2
Arterial_1
Macrophage1
Peripheral_Nerve_1
Acinar
Ductal
CCL2+_sub1
Prol.2
SFRP1+_sub2
Prol.4
SFRP1+_sub1
SFRP2+
Prol.3
FEV+High
Pre-Alpha
Pre-Beta
Epsilon
Delta
EP
Alpha
Pre-Acinar
Pre-Ductal
Exocrine_Prol1
Exocrine_Prol2
FGF9 – FGFR2
Ductal
Pre-Ductal
Mesothelial
Exocrine_Prol1
Exocrine_Prol2
FGF9 – FGFR3
Ductal
Pre-Ductal
Mesothelial
Exocrine_Prol1
Exocrine_Prol2
FGF9 – FGFR4
Ductal
Acinar
Pre-Acinar
Mesothelial
Pre-Ductal
Exocrine_Prol2
Exocrine_Prol1

Figure 8. Elucidation of *FGF9* and *FGFR* expression, and prediction of ligand-receptor interactions, in the developing human pancreas

(A) UMAP of the sub-clustered mesenchymal compartment of an integrated scRNA-Seq dataset of cells from human fetal pancreas (HFP) comprising 8 individuals across developmental stages 8–20 weeks post conception (wpc). The feature plots inset to the right depict the expression of *FGF9* and the mesothelial cell markers *KRT19, WT1,* and *MSLN* in the mesothelial population. Dataset, cell clustering, and annotations were adopted from de la O, et al.[73]

(B) Stacked violin plot shows the expression levels of *FGF9* and *FGFR1-4* in each mesenchymal sub-subpopulation shown in (A).

(C) *In situ* hybridization/immunofluorescence staining (ISH/IF) for KRT19 protein (green) to mark duct and mesothelium, *WT1* transcript (red) to mark mesothelium, and *FGF9* transcript (magenta). Nuclei were counterstained with DAPI (blue). Dashed yellow lines outline the mesothelial layer. White rectangles outline regions of interest, magnified in the inset, showing KRT19+/WT1+ mesothelial cells that also express *FGF9*. Scale bar is 50 μm.

(D–G) ISH/IF staining of 9 wpc human fetal pancreas tissue detecting *FGFR1-4* transcripts (magenta), Vimentin (VIM; green) to mark mesenchymal cells, and KRT19 (gray) to mark the ductal trunk epithelium and mesothelium reveals expression of (D) *FGFR1* in mesenchyme and duct; (E) *FGFR2* in duct; (F) *FGFR3* in duct; and (G) *FGFR4* in duct. Dashed gray lines outline the KRT19+ ductal trunk. Nuclei were counterstained with DAPI. Scale bars are 50 μm.

(H) CellChat analysis predicts the relative contribution of each FGF9-FGFR signaling pair to the overall FGF9 signaling active within the merged dataset of human fetal pancreas from 8 to 20 wpc.

(I) Circle plots show the cell type-specific signaling predicted for each FGF9-FGFR ligand-receptor pair, across all populations in which signaling is predicted to occur for that pair. Line thickness is proportional to signaling strength, and line colors represent which population is annotated as the "Sender" of FGF9 signal.

mesothelial layer, we used *WT1*, a known marker of mesothelial cells, with KRT19, which marks both mesothelium and ductal cells. We observed co-expression of *WT1* and *FGF9* in KRT19+ mesothelium (Figure 8C), with rare *FGF9* signal in a small proportion of PDX1+KRT19+ ductal cells (Figure S9D). *FGFR1* was enriched in pancreatic mesenchymal and ductal tissues (Figure 8D), which corroborates the computational analysis of *FGFR1* expression in the human fetal pancreas scRNA-Seq dataset (Figures 8B, S9B, and S9C). In contrast, *FGFR2-4* were detected in KRT19+ ductal cells (Figures 8E–8G). The expression patterns of *FGF9* and *FGFRs* in the mesenchyme of the developing human pancreas are similar our findings in the developing mouse pancreas, suggesting that FGF9 may regulate human pancreatic mesenchymal development through *FGFR1* rather than *FGFR2-4*.

We applied CellChat to the integrated human fetal pancreas scRNA-Seq dataset to interpret the FGF9-FGFR signaling networks across 8 to 20 wpc (Figures 8H and 8I). Similar to what we observed in the developing mouse pancreas, in human tissues, FGF9-FGFR1 was also predicted to have the highest relative contribution to overall FGF9 signaling compared to FGF9-FGFR2/3/4 ligand-receptor pairs (Figure 8H). Circle Plots further predicted the specific "Sender" and "Receiver" cell types for each signaling pair (Figure 8I). Mesothelium was interpreted as the strongest "Sender" of FGF9, with a relatively low contribution of FGF9 secretion from exocrine populations (Ductal, Exocrine_Prolif.1, Exocrine_Polif.2) (Figure 8I). Taken together, these results predict that in human tissue FGF9 secreted by mesothelium functions signals to a broad population of cells expressing FGFR1, and to exocrine cells through FGFR2-4.

In summary, our data reveal a similarity in the FGF9-FGFR expression profiles and signaling crosstalk between mouse and human, suggesting conservation of Fgf9 function in mouse and human pancreatic development. The role of FGF9 in human pancreatic mesenchymal fate specification warrants future investigation.

DISCUSSION

A number of studies have advanced our understanding of the role of inductive signaling from mesoderm-derived tissues in regulating pancreatic endoderm.[14–16,21,23,25,26,29,31,74–78] In our previous work using scRNA-Seq to study mouse pancreas development, we found that the specialized mesenchymal cell type called mesothelium expresses multiple secreted factors that may impact pancreatic organogenesis; among the factors most specific for mesothelial expression at E12.5 was *Fgf9*.[37] In this study, we report that Fgf9 is required for proper formation and development of multiple gut organs, including the pancreas, spleen, and stomach.

There appear to be key distinctions between the phenotypes observed for embryos mutant for *Fgf9* versus *Fgf10,* another mesenchymally-expressed, secreted factor reported to play a role in pancreatic development.[31] *Fgf10* null embryos do not display the asplenia we observed in *Fgf9* null embryos. In both genotypes, there is a reduction in the number of pancreatic progenitors at E10.5, although in *Fgf10* mutants this is believed to be because of a significant reduction in progenitor proliferation. Conversely, in *Fgf9* mutants we did not observe a reduction in proliferation of pancreatic progenitors. Our *in situ* hybridization data revealed regions in which expression of *Fgf9* and *Fgf10* are spatially distinct, as well as regions where they are overlapping, in early pancreatic mesenchyme. Although *Fgf10* null pancreata display an almost

complete loss of islets, in contrast the loss of Fgf9 does not result in loss of any major cell lineage. Future studies using mouse genetic tools can further clarify which functions of Fgf9 and Fgf10 are redundant or distinct in mouse pancreatic development.

Loss of Fgf9 appears to predominantly affect mesenchymal formation and gene expression programs. By E11.5, there is an obvious reduction in condensing mesenchyme surrounding the dorsal bud, and this is at least partially attributable to a reduction in proliferation, initially of mesenchymal cells and then of epithelial cells. Our findings of reduced mesenchymal area and proliferation on loss of Fgf9 are consistent with previous observations in *Fgf9* null lung tissue.[43,79–81] At E13.5 and E14.5, our bulk and single-cell RNA-Seq studies revealed that loss of Fgf9 led to reduced expression of multiple genes reported to mark spleno-pancreatic mesenchymal progenitors, including *Tlx1*, *Barx1*, *Nkx3.2,* and *Nkx2.5*.[17,19,50–52,55–57,82,83] Future studies refining the connections between Fgf9 and these homeobox transcription factors, for instance by employing single- and multi-gene knockout studies, will provide valuable insights into the molecular mechanisms downstream of Fgf9 signaling in the pancreas. It is very possible that the initial defects in mesenchymal proliferation have downstream, compounding locoregional effects on ensuing mesenchymal development. In addition, initial defects in mesenchymal tissue growth may result in altered contact with other mesenchymal or epithelial populations from which they normally receive important growth cues.

Based on the expression patterns of *Fgf9* and *Fgfrs* in our studies, it is likely that in murine pancreas mesenchymally-derived FGF9 transduces signals primarily through FGFR1 around E10.5, and then epithelially-derived FGF9 acts through FGFR3 at later timepoints. This would be consistent with Fgf9 signaling in the developing lung,[79,80,84] although further functional studies are needed to confirm this model. Our expression data presented here are limited by the fact that we did not use probes to differentiate between the *Fgfr IIIb* and *IIIc* splice variants, which are critical determinants of ligand binding specificity. Teasing out the role of each Fgf9-Fgfr pair in pancreatic development awaits further experimental validation using transgenic mouse lines.

In addition to characterizing the expression of *Fgf9* and its cognate receptors in the developing mouse pancreas, we have also assessed the expression of *FGF9* and the *FGF* receptors in the developing human pancreas from 8 to 20 wpc. Our scRNA-Seq data and confirmatory staining in independent tissue sections revealed that consistent with mouse, mesothelial cells are the major population that robustly expresses *FGF9* in the human fetal pancreas. Among the FGFRs, *FGFR1* is broadly expressed in the human pancreatic tissue, whereas *FGFR2-4* expression is restricted to KRT19+ ductal cells. Our data suggest that our findings in murine tissue of mesothelial expression of *FGF9* do extend to human tissue, as well, and that FGF9 may play a similar role in fetal pancreatic development in humans. Future work employing explant culture of human fetal tissue at various developmental stages with addition of recombinant human FGF9 protein and/or small molecule inhibitors or activators of specific FGF receptors could further investigate the function of FGF signaling in human fetal pancreatic development.

Limitations of the study

We report here that loss of Fgf9 results in changes in pancreatic gene expression at E13.5 and E14.5, but one caveat of these results is that these changes could be direct or indirect. Although we attempted to apply bulk- and scRNA-Seq techniques to investigate alterations in cellular composition and identity in *Fgf9* null embryos at early timepoints corresponding to when pancreatic progenitors are reduced (i.e., E10.5), these studies proved infeasible because of significant technical challenges relating to extremely limiting number of cells. Future work to investigate transcriptional and population changes at such early timepoints will be informative once technical advances render it experimentally feasible.

Given the expression of *Fgf9* that we observed in mesenchyme in early development and in rare ductal cells at E14.5 and E17.5, it remains unclear whether the pancreatic phenotype in *Fgf9* null embryos is caused solely by the loss of secreted FGF9 from the mesothelial compartment, the mesenchymal compartment, the ductal compartment, or a combination of the above. To address this question, cell type-specific knockouts using epithelial-, mesenchymal-, and ideally mesothelial-specific Cre lines are warranted. Such an approach could also address a caveat with our current mouse model, which entails the use of a whole-body knockout of *Fgf9*. Pdx1-Cre-mediated excision of *Fgf9*, for instance, would reveal epithelial mediated functions of FGF9, if any, in the foregut region (where *Pdx1* is expressed in pancreas, stomach, and duodenum) as opposed to throughout the body. The field of mesenchyme biology has been relatively

hampered by the dearth of tissue-specific mesenchyme gene markers or corresponding Cre lines (e.g., a Cre driver line specific to pancreatic mesothelium versus mesothelia in other organs). Given the dynamic expression of *Fgf9* across developmental time in different cell types, it would also be interesting to perform temporally controlled deletion with inducible Cre-mediated excision of *Fgf9* as well. Similarly, the underlying mechanisms contributing to the spleen and stomach phenotypes in *Fgf9* null embryos require tissue-specific investigation in the future.

STAR★METHODS

Detailed methods are provided in the online version of this paper and include the following:

- KEY RESOURCES TABLE
- RESOURCE AVAILABILITY
  - Lead contact
  - Materials availability
  - Data and code availability
- EXPERIMENTAL MODEL AND SUBJECT DETAILS
  - Animals
- METHOD DETAILS
  - Histology, immunofluorescence, and imaging of mouse tissue
  - Whole-mount staining
  - Histology, immunofluorescence, and staining of human tissue
  - *In situ* hybridization
  - Bulk RNA-Sequencing and analysis
  - Preparation of tissue for single-cell RNA-Sequencing
  - Mouse single-cell capture and sequencing
  - Analysis of mouse single-cell RNA-Sequencing data
  - Analysis of human single-cell RNA-Sequencing data
  - Quantification of pancreatic cellular communication with CellChat
- QUANTIFICATION AND STATISTICAL ANALYSIS
  - Quantification of PDX1+ cells in dorsal pancreas
  - Analysis of cellular proliferation
  - Quantification and statistical analysis of endocrine populations

SUPPLEMENTAL INFORMATION

Supplemental information can be found online at https://doi.org/10.1016/j.isci.2023.106500.

ACKNOWLEDGMENTS

This work was supported by grants to J.B.S. from the NIH (R01DK118421), the Nora Eccles Treadwell Foundation, the UCSF Resource Allocation Program, and the UCSF Program for Breakthrough Biomedical Research, which is partially funded by the Sandler Foundation. Support to D.M.O. was provided by NIH grant R01HL154747. S.P. was supported by the Kraft Family Fellowship to the UCSF Diabetes Center, the UCSF Division of Endocrinology and Metabolism, and the UCSF Diabetes and Endocrinology Fellowship Program, supported by NIH T32 DK007418. Z.L. was supported by the Jeffrey G. Klein Family Diabetes Fellowship to the UCSF Diabetes Center. S.M.D. was supported by the UCSF Discovery Fellows Program, the Kraft Family Fellowship to the UCSF Diabetes Center, NIH NIGMS IMSD Grant #R25GM056847-23, and NIH/NIDDK diversity supplement R01DK118421-02S1. L.E.B. was supported by an Achievement Rewards for College Scientists (ARCS) Foundation Scholar Award.

The authors would like to acknowledge expert technical assistance from the UCSF Broad Imaging Core, the UCSF Parnassus Flow Cytometry Core, and the UCSF Institute for Human Genetics Core. We are grateful to Dr. Jeffrey Bush, Dr. Teng Teng, and Dr. Camilla Teng for technical advice on cleaved caspase-3 staining, and to Xinkai Yao for assistance with animal husbandry.

AUTHOR CONTRIBUTIONS

S.P.: Conceptualization, Validation, Formal analysis, Investigation, Data Curation, Writing – Original Draft, Writing – Review and Editing, Visualization.

Z.L.: Conceptualization, Software, Validation, Formal analysis, Investigation, Data Curation, Writing – Original Draft, Writing – Review and Editing, Visualization.

S.d.l.O.: Conceptualization, Software, Formal analysis, Investigation, Data Curation, Visualization.

S.C.: Validation, Investigation.

L.E.B.: Conceptualization, Investigation.

X.Z.: Investigation, Visualization.

D.M.O.: Resources, Writing – Review and Editing.

J.B.S.: Conceptualization, Resources, Writing – Original Draft, Writing – Review and Editing, Supervision, Project administration, Funding acquisition.

DECLARATION OF INTERESTS

The authors declare no competing interests.

Received: August 11, 2022
Revised: December 21, 2022
Accepted: March 22, 2023
Published: March 25, 2023

REFERENCES

1. Simsek, S., Zhou, T., Robinson, C.L., Tsai, S.-Y., Crespo, M., Amin, S., Lin, X., Hon, J., Evans, T., and Chen, S. (2016). Modeling cystic fibrosis using pluripotent stem cell-derived human pancreatic ductal epithelial cells. Stem Cells Transl. Med. *5*, 572–579. https://doi.org/10.5966/sctm.2015-0276.

2. Rezania, A., Bruin, J.E., Arora, P., Rubin, A., Batushansky, I., Asadi, A., O'Dwyer, S., Quiskamp, N., Mojibian, M., Albrecht, T., et al. (2014). Reversal of diabetes with insulin-producing cells derived in vitro from human pluripotent stem cells. Nat. Biotechnol. *32*, 1121–1133. https://doi.org/10.1038/nbt.3033.

3. Pagliuca, F.W., Millman, J.R., Gürtler, M., Segel, M., Van Dervort, A., Ryu, J.H., Peterson, Q.P., Greiner, D., and Melton, D.A. (2014). Generation of functional human pancreatic β cells in vitro. Cell *159*, 428–439. https://doi.org/10.1016/j.cell.2014.09.040.

4. Migliorini, A., Nostro, M.C., and Sneddon, J.B. (2021). Human pluripotent stem cell-derived insulin-producing cells: a regenerative medicine perspective. Cell Metabol. *33*, 721–731. https://doi.org/10.1016/j.cmet.2021.03.021.

5. Russ, H.A., Parent, A.V., Ringler, J.J., Hennings, T.G., Nair, G.G., Shveygert, M., Guo, T., Puri, S., Haataja, L., Cirulli, V., et al. (2015). Controlled induction of human pancreatic progenitors produces functional beta-like cells in vitro. EMBO J. *34*, 1759–1772. https://doi.org/10.15252/embj.201591058.

6. Peterson, Q.P., Veres, A., Chen, L., Slama, M.Q., Kenty, J.H.R., Hassoun, S., Brown, M.R., Dou, H., Duffy, C.D., Zhou, Q., et al. (2020). A method for the generation of human stem cell-derived alpha cells. Nat. Commun. *11*, 2241. https://doi.org/10.1038/s41467-020-16049-3.

7. Rezania, A., Riedel, M.J., Wideman, R.D., Karanu, F., Ao, Z., Warnock, G.L., and Kieffer, T.J. (2011). Production of functional glucagon-secreting α-cells from human embryonic stem cells. Diabetes *60*, 239–247. https://doi.org/10.2337/db10-0573.

8. D'Amour, K.A., Bang, A.G., Eliazer, S., Kelly, O.G., Agulnick, A.D., Smart, N.G., Moorman, M.A., Kroon, E., Carpenter, M.K., and Baetge, E.E. (2006). Production of pancreatic hormone-expressing endocrine cells from human embryonic stem cells. Nat. Biotechnol. *24*, 1392–1401. https://doi.org/10.1038/nbt1259.

9. Kroon, E., Martinson, L.A., Kadoya, K., Bang, A.G., Kelly, O.G., Eliazer, S., Young, H., Richardson, M., Smart, N.G., Cunningham, J., et al. (2008). Pancreatic endoderm derived from human embryonic stem cells generates glucose-responsive insulin-secreting cells in vivo. Nat. Biotechnol. *26*, 443–452. https://doi.org/10.1038/nbt1393.

10. Huang, L., Holtzinger, A., Jagan, I., BeGora, M., Lohse, I., Ngai, N., Nostro, C., Wang, R., Muthuswamy, L.B., Crawford, H.C., et al. (2015). Ductal pancreatic cancer modeling and drug screening using human pluripotent stem cell- and patient-derived tumor organoids. Nat. Med. *21*, 1364–1371. https://doi.org/10.1038/nm.3973.

11. Hohwieler, M., Illing, A., Hermann, P.C., Mayer, T., Stockmann, M., Perkhofer, L., Eiseler, T., Antony, J.S., Müller, M., Renz, S., et al. (2017). Human pluripotent stem cell-derived acinar/ductal organoids generate human pancreas upon orthotopic transplantation and allow disease modelling. Gut *66*, 473–486. https://doi.org/10.1136/gutjnl-2016-312423.

12. Gaertner, B., Carrano, A.C., and Sander, M. (2019). Human stem cell models: lessons for pancreatic development and disease. Genes Dev. *33*, 1475–1490. https://doi.org/10.1101/gad.331397.119.

13. Kim, S.K., Hebrok, M., and Melton, D.A. (1997). Notochord to endoderm signaling is required for pancreas development. Development *124*, 4243–4252. https://doi.org/10.1242/dev.124.21.4243.

14. Kumar, M., Jordan, N., Melton, D., and Grapin-Botton, A. (2003). Signals from lateral plate mesoderm instruct endoderm toward a pancreatic fate. Dev. Biol. *259*, 109–122. https://doi.org/10.1016/s0012-1606(03)00183-0.

15. Lammert, E., Cleaver, O., and Melton, D. (2001). Induction of pancreatic differentiation by signals from blood vessels. Science *294*, 564–567. https://doi.org/10.1126/science.1064344.

16. Yoshitomi, H., and Zaret, K.S. (2004). Endothelial cell interactions initiate dorsal pancreas development by selectively inducing the transcription factor Ptf1a. Development *131*, 807–817. https://doi.org/10.1242/dev.00960.

17. Asayesh, A., Sharpe, J., Watson, R.P., Hecksher-Sørensen, J., Hastie, N.D., Hill, R.E.,

and Ahlgren, U. (2006). Spleen versus pancreas: strict control of organ interrelationship revealed by analyses of Bapx1-/- mice. Genes Dev. *20*, 2208–2213. https://doi.org/10.1101/gad.381906.

18. Byrnes, K.G., Walsh, D., Walsh, L.G., Coffey, D.M., Ullah, M.F., Mirapeix, R., Hikspoors, J., Lamers, W., Wu, Y., Zhang, X.-Q., et al. (2021). The development and structure of the mesentery. Commun. Biol. *4*, 982. https://doi.org/10.1038/s42003-021-02496-1.

19. Hecksher-Sørensen, J., Watson, R.P., Lettice, L.A., Serup, P., Eley, L., De Angelis, C., Ahlgren, U., and Hill, R.E. (2004). The splanchnic mesodermal plate directs spleen and pancreatic laterality, and is regulated by Bapx1/Nkx3.2. Development *131*, 4665–4675. https://doi.org/10.1242/dev.01364.

20. Green, M.C. (1967). A defect of the splanchnic mesoderm caused by the mutant gene dominant hemimelia in the mouse. Dev. Biol. *15*, 62–89. https://doi.org/10.1016/0012-1606(67)90006-1.

21. Landsman, L., Nijagal, A., Whitchurch, T.J., Vanderlaan, R.L., Zimmer, W.E., Mackenzie, T.C., and Hebrok, M. (2011). Pancreatic mesenchyme regulates epithelial organogenesis throughout development. PLoS Biol. *9*, e1001143. https://doi.org/10.1371/journal.pbio.1001143.

22. Golosow, N., and Grobstein, C. (1962). Epitheliomesenchymal interaction in pancreatic morphogenesis. Dev. Biol. *4*, 242–255. https://doi.org/10.1016/0012-1606(62)90042-8.

23. Gittes, G.K., Galante, P.E., Hanahan, D., Rutter, W.J., and Debase, H.T. (1996). Lineage-specific morphogenesis in the developing pancreas: role of mesenchymal factors. Development *122*, 439–447. https://doi.org/10.1242/dev.122.2.439.

24. Attali, M., Stetsyuk, V., Basmaciogullari, A., Aiello, V., Zanta-Boussif, M.A., Duvillie, B., and Scharfmann, R. (2007). Control of beta-cell differentiation by the pancreatic mesenchyme. Diabetes *56*, 1248–1258. https://doi.org/10.2337/db06-1307.

25. Larsen, B.M., Hrycaj, S.M., Newman, M., Li, Y., and Wellik, D.M. (2015). Mesenchymal Hox6 function is required for mouse pancreatic endocrine cell differentiation. Development *142*, 3859–3868. https://doi.org/10.1242/dev.126888.

26. Cozzitorto, C., Mueller, L., Ruzittu, S., Mah, N., Willnow, D., Darrigrand, J.-F., Wilson, H., Khosravinia, D., Mahmoud, A.-A., Risolino, M., et al. (2020). A specialized niche in the pancreatic microenvironment promotes endocrine differentiation. Dev. Cell *55*, 150–162.e6. https://doi.org/10.1016/j.devcel.2020.08.003.

27. Arregi, I., Climent, M., Iliev, D., Strasser, J., Gouignard, N., Johansson, J.K., Singh, T., Mazur, M., Semb, H., Artner, I., et al. (2016). Retinol dehydrogenase-10 regulates pancreas organogenesis and endocrine cell differentiation via paracrine retinoic Acid signaling. Endocrinology *157*, 4615–4631. https://doi.org/10.1210/en.2016-1745.

28. Jonckheere, N., Mayes, E., Shih, H.-P., Li, B., Lioubinski, O., Dai, X., and Sander, M. (2008). Analysis of mPygo2 mutant mice suggests a requirement for mesenchymal Wnt signaling in pancreatic growth and differentiation. Dev. Biol. *318*, 224–235. https://doi.org/10.1016/j.ydbio.2008.03.014.

29. Ahnfelt-Rønne, J., Ravassard, P., Pardanaud-Glavieux, C., Scharfmann, R., and Serup, P. (2010). Mesenchymal bone morphogenetic protein signaling is required for normal pancreas development. Diabetes *59*, 1948–1956. https://doi.org/10.2337/db09-1010.

30. Dichmann, D.S., Miller, C.P., Jensen, J., Scott Heller, R., and Serup, P. (2003). Expression and misexpression of members of the FGF and TGFbeta families of growth factors in the developing mouse pancreas. Dev. Dynam. *226*, 663–674. https://doi.org/10.1002/dvdy.10270.

31. Bhushan, A., Itoh, N., Kato, S., Thiery, J.P., Czernichow, P., Bellusci, S., and Scharfmann, R. (2001). Fgf10 is essential for maintaining the proliferative capacity of epithelial progenitor cells during early pancreatic organogenesis. Development *128*, 5109–5117. https://doi.org/10.1242/dev.128.24.5109.

32. Hart, A., Papadopoulou, S., and Edlund, H. (2003). Fgf10 maintains notch activation, stimulates proliferation, and blocks differentiation of pancreatic epithelial cells. Dev. Dynam. *228*, 185–193. https://doi.org/10.1002/dvdy.10368.

33. Miralles, F., Lamotte, L., Couton, D., and Joshi, R.L. (2006). Interplay between FGF10 and Notch signalling is required for the self-renewal of pancreatic progenitors. Int. J. Dev. Biol. *50*, 17–26. https://doi.org/10.1387/ijdb.052080fm.

34. Sylvestersen, K.B., Herrera, P.L., Serup, P., and Rescan, C. (2011). Fgf9 signalling stimulates Spred and Sprouty expression in embryonic mouse pancreas mesenchyme. Gene Expr. Patterns *11*, 105–111. https://doi.org/10.1016/j.gep.2010.10.001.

35. Ornitz, D.M., and Itoh, N. (2022). New developments in the biology of fibroblast growth factors. WIREs Mech. Dis. *14*, e1549. https://doi.org/10.1002/wsbm.1549.

36. Colvin, J.S., Feldman, B., Nadeau, J.H., Goldfarb, M., and Ornitz, D.M. (1999). Genomic organization and embryonic expression of the mouse fibroblast growth factor 9 gene. Dev. Dynam. *216*, 72–88. https://doi.org/10.1002/(SICI)1097-0177(199909)216:1<72::AID-DVDY9>3.0.CO;2-9.

37. Byrnes, L.E., Wong, D.M., Subramaniam, M., Meyer, N.P., Gilchrist, C.L., Knox, S.M., Tward, A.D., Ye, C.J., and Sneddon, J.B. (2018). Lineage dynamics of murine pancreatic development at single-cell resolution. Nat. Commun. *9*, 3922. https://doi.org/10.1038/s41467-018-06176-3.

38. Sakhneny, L., Khalifa-Malka, L., and Landsman, L. (2019). Pancreas organogenesis: approaches to elucidate the role of epithelial-mesenchymal interactions. Semin. Cell Dev. Biol. *92*, 89–96. https://doi.org/10.1016/j.semcdb.2018.08.012.

39. Villasenor, A., Chong, D.C., Henkemeyer, M., and Cleaver, O. (2010). Epithelial dynamics of pancreatic branching morphogenesis. Development *137*, 4295–4305. https://doi.org/10.1242/dev.052993.

40. Winters, N., and Bader, D. (2013). Development of the serosal mesothelium. J. Dev. Biol. *1*, 64–81. https://doi.org/10.3390/jdb1020064.

41. Herrick, S.E., and Mutsaers, S.E. (2004). Mesothelial progenitor cells and their potential in tissue engineering. Int. J. Biochem. Cell Biol. *36*, 621–642. https://doi.org/10.1016/j.biocel.2003.11.002.

42. Quijada, P., Trembley, M.A., and Small, E.M. (2020). The role of the epicardium during heart development and repair. Circ. Res. *126*, 377–394. https://doi.org/10.1161/CIRCRESAHA.119.315857.

43. Colvin, J.S., White, A.C., Pratt, S.J., and Ornitz, D.M. (2001). Lung hypoplasia and neonatal death in Fgf9-null mice identify this gene as an essential regulator of lung mesenchyme. Development *128*, 2095–2106. https://doi.org/10.1242/dev.128.11.2095.

44. Onitsuka, I., Tanaka, M., and Miyajima, A. (2010). Characterization and functional analyses of hepatic mesothelial cells in mouse liver development. Gastroenterology *138*, 1525–1535. https://doi.org/10.1053/j.gastro.2009.12.059.

45. Gittes, G.K. (2009). Developmental biology of the pancreas: a comprehensive review. Dev. Biol. *326*, 4–35. https://doi.org/10.1016/j.ydbio.2008.10.024.

46. Ornitz, D.M., Xu, J., Colvin, J.S., McEwen, D.G., MacArthur, C.A., Coulier, F., Gao, G., and Goldfarb, M. (1996). Receptor specificity of the fibroblast growth factor family. J. Biol. Chem. *271*, 15292–15297. https://doi.org/10.1074/jbc.271.25.15292.

47. Ornitz, D.M., and Itoh, N. (2015). The fibroblast growth factor signaling pathway. Wiley Interdiscip. Rev. Dev. Biol. *4*, 215–266. https://doi.org/10.1002/wdev.176.

48. Zhang, X., Ibrahimi, O.A., Olsen, S.K., Umemori, H., Mohammadi, M., and Ornitz, D.M. (2006). Receptor specificity of the fibroblast growth factor family. The complete mammalian FGF family. J. Biol. Chem. *281*, 15694–15700. https://doi.org/10.1074/jbc.M601252200.

49. Huh, S.-H., Warchol, M.E., and Ornitz, D.M. (2015). Cochlear progenitor number is controlled through mesenchymal FGF receptor signaling. Elife *4*, e05921. https://doi.org/10.7554/eLife.05921.

50. Roberts, C.W., Sonder, A.M., Lumsden, A., and Korsmeyer, S.J. (1995). Development expression of Hox11 and specification of splenic cell fate. Am. J. Pathol. *146*, 1089–1101.

51. Roberts, C.W., Shutter, J.R., and Korsmeyer, S.J. (1994). Hox11 controls the genesis of the

spleen. Nature *368*, 747–749. https://doi.org/10.1038/368747a0.

52. Dear, T.N., Colledge, W.H., Carlton, M.B., Lavenir, I., Larson, T., Smith, A.J., Warren, A.J., Evans, M.J., Sofroniew, M.V., and Rabbitts, T.H. (1995). The Hox11 gene is essential for cell survival during spleen development. Development *121*, 2909–2915. https://doi.org/10.1242/dev.121.9.2909.

53. Jayewickreme, C.D., and Shivdasani, R.A. (2015). Control of stomach smooth muscle development and intestinal rotation by transcription factor BARX1. Dev. Biol. *405*, 21–32. https://doi.org/10.1016/j.ydbio.2015.05.024.

54. Kim, B.-M., Miletich, I., Mao, J., McMahon, A.P., Sharpe, P.A., and Shivdasani, R.A. (2007). Independent functions and mechanisms for homeobox gene Barx1 in patterning mouse stomach and spleen. Development *134*, 3603–3613. https://doi.org/10.1242/dev.009308.

55. Koss, M., Bolze, A., Brendolan, A., Saggese, M., Capellini, T.D., Bojilova, E., Boisson, B., Prall, O.W.J., Elliott, D.A., Solloway, M., et al. (2012). Congenital asplenia in mice and humans with mutations in a Pbx/Nkx2-5/p15 module. Dev. Cell *22*, 913–926. https://doi.org/10.1016/j.devcel.2012.02.009.

56. Castagnaro, L., Lenti, E., Maruzzelli, S., Spinardi, L., Migliori, E., Farinello, D., Sitia, G., Harrelson, Z., Evans, S.M., Guidotti, L.G., et al. (2013). Nkx2-5(+)islet1(+) mesenchymal precursors generate distinct spleen stromal cell subsets and participate in restoring stromal network integrity. Immunity *38*, 782–791. https://doi.org/10.1016/j.immuni.2012.12.005.

57. Tribioli, C., and Lufkin, T. (1999). The murine Bapx1 homeobox gene plays a critical role in embryonic development of the axial skeleton and spleen. Development *126*, 5699–5711.

58. Ottolenghi, C., Moreira-Filho, C., Mendonça, B.B., Barbieri, M., Fellous, M., Berkovitz, G.D., and McElreavey, K. (2001). Absence of mutations involving the LIM homeobox domain gene LHX9 in 46,XY gonadal agenesis and dysgenesis. J. Clin. Endocrinol. Metab. *86*, 2465–2469. https://doi.org/10.1210/jcem.86.6.7539.

59. Birk, O.S., Casiano, D.E., Wassif, C.A., Cogliati, T., Zhao, L., Zhao, Y., Grinberg, A., Huang, S., Kreidberg, J.A., Parker, K.L., et al. (2000). The LIM homeobox gene Lhx9 is essential for mouse gonad formation. Nature *403*, 909–913. https://doi.org/10.1038/35002622.

60. Tandon, P., Wilczewski, C.M., Williams, C.E., and Conlon, F.L. (2016). The Lhx9-integrin pathway is essential for positioning of the proepicardial organ. Development *143*, 831–840. https://doi.org/10.1242/dev.129551.

61. Bertuzzi, S., Porter, F.D., Pitts, A., Kumar, M., Agulnick, A., Wassif, C., and Westphal, H. (1999). Characterization of Lhx9, a novel LIM/homeobox gene expressed by the pioneer neurons in the mouse cerebral cortex. Mech. Dev. *81*, 193–198. https://doi.org/10.1016/s0925-4773(98)00233-0.

62. Kim, J.Y., Manna, D., Etscheid, M., Leergaard, T.B., and Kanse, S.M. (2022). Differential regulation of *lhx9* expression in mouse and chicken limbs. Faseb. J. *36*, e22564. https://doi.org/10.1096/fasebj.2022.36.S1.R3263.

63. Atkinson-Leadbeater, K., Bertolesi, G.E., Johnston, J.A., Hehr, C.L., and McFarlane, S. (2009). FGF receptor dependent regulation of Lhx9 expression in the developing nervous system. Dev. Dynam. *238*, 367–375. https://doi.org/10.1002/dvdy.21850.

64. Yang, Y., and Wilson, M.J. (2015). Lhx9 gene expression during early limb development in mice requires the FGF signalling pathway. Gene Expr. Patterns *19*, 45–51. https://doi.org/10.1016/j.gep.2015.07.002.

65. Leavitt, T., Hu, M.S., Borrelli, M.R., Januszyk, M., Garcia, J.T., Ransom, R.C., Mascharak, S., desJardins-Park, H.E., Litzenburger, U.M., Walmsley, G.G., et al. (2020). Prrx1 fibroblasts represent a pro-fibrotic lineage in the mouse ventral dermis. Cell Rep. *33*, 108356. https://doi.org/10.1016/j.celrep.2020.108356.

66. Soldatov, R., Kaucka, M., Kastriti, M.E., Petersen, J., Chontorotzea, T., Englmaier, L., Akkuratova, N., Yang, Y., Häring, M., Dyachuk, V., et al. (2019). Spatiotemporal structure of cell fate decisions in murine neural crest. Science *364*, eaas9536. https://doi.org/10.1126/science.aas9536.

67. Müller, I., Rössler, O.G., Wittig, C., Menger, M.D., and Thiel, G. (2012). Critical role of Egr transcription factors in regulating insulin biosynthesis, blood glucose homeostasis, and islet size. Endocrinology *153*, 3040–3053. https://doi.org/10.1210/en.2012-1064.

68. Thiel, G., Müller, I., and Rössler, O.G. (2014). Expression, signaling and function of Egr transcription factors in pancreatic β-cells and insulin-responsive tissues. Mol. Cell. Endocrinol. *388*, 10–19. https://doi.org/10.1016/j.mce.2014.03.001.

69. Vanhorenbeeck, V., Jenny, M., Cornut, J.-F., Gradwohl, G., Lemaigre, F.P., Rousseau, G.G., and Jacquemin, P. (2007). Role of the Onecut transcription factors in pancreas morphogenesis and in pancreatic and enteric endocrine differentiation. Dev. Biol. *305*, 685–694. https://doi.org/10.1016/j.ydbio.2007.02.027.

70. Yu, K.S., Frumm, S.M., Park, J.S., Lee, K., Wong, D.M., Byrnes, L., Knox, S.M., Sneddon, J.B., and Tward, A.D. (2019). Development of the mouse and human cochlea at single cell resolution. Preprint at bioRxiv. https://doi.org/10.1101/739680.

71. Rust, K., Byrnes, L.E., Yu, K.S., Park, J.S., Sneddon, J.B., Tward, A.D., and Nystul, T.G. (2020). A single-cell atlas and lineage analysis of the adult Drosophila ovary. Nat. Commun. *11*, 5628. https://doi.org/10.1038/s41467-020-19361-0.

72. Jin, S., Guerrero-Juarez, C.F., Zhang, L., Chang, I., Ramos, R., Kuan, C.-H., Myung, P., Plikus, M.V., and Nie, Q. (2021). Inference and analysis of cell-cell communication using CellChat. Nat. Commun. *12*, 1088. https://doi.org/10.1038/s41467-021-21246-9.

73. de la, O.S., Liu, Z., Sun, H., Yu, S.K., Wong, D.M., Chu, E., Rao, S.A., Eng, N., Peixoto, G., Bouza, J., et al. (2022). Single-cell multi-omic roadmap of human fetal pancreatic development. Preprint at. bioRxiv. https://doi.org/10.1101/2022.02.17.480942.

74. Tulachan, S.S., Doi, R., Hirai, Y., Kawaguchi, Y., Koizumi, M., Hembree, M., Tei, E., Crowley, A., Yew, H., McFall, C., et al. (2006). Mesenchymal epimorphin is important for pancreatic duct morphogenesis. Dev. Growth Differ. *48*, 65–72. https://doi.org/10.1111/j.1440-169X.2006.00846.x.

75. Seymour, P.A., Shih, H.P., Patel, N.A., Freude, K.K., Xie, R., Lim, C.J., and Sander, M. (2012). A Sox9/Fgf feed-forward loop maintains pancreatic organ identity. Development *139*, 3363–3372. https://doi.org/10.1242/dev.078733.

76. Li, Z., Manna, P., Kobayashi, H., Spilde, T., Bhatia, A., Preuett, B., Prasadan, K., Hembree, M., and Gittes, G.K. (2004). Multifaceted pancreatic mesenchymal control of epithelial lineage selection. Dev. Biol. *269*, 252–263. https://doi.org/10.1016/j.ydbio.2004.01.043.

77. Duvillié, B., Attali, M., Bounacer, A., Ravassard, P., Basmaciogullari, A., and Scharfmann, R. (2006). The mesenchyme controls the timing of pancreatic beta-cell differentiation. Diabetes *55*, 582–589. https://doi.org/10.2337/diabetes.55.03.06.db05-0839.

78. Stafford, D., White, R.J., Kinkel, M.D., Linville, A., Schilling, T.F., and Prince, V.E. (2006). Retinoids signal directly to zebrafish endoderm to specify insulin-expressing beta-cells. Development *133*, 949–956. https://doi.org/10.1242/dev.02263.

79. Yin, Y., Wang, F., and Ornitz, D.M. (2011). Mesothelial- and epithelial-derived FGF9 have distinct functions in the regulation of lung development. Development *138*, 3169–3177. https://doi.org/10.1242/dev.065110.

80. Yin, Y., White, A.C., Huh, S.-H., Hilton, M.J., Kanazawa, H., Long, F., and Ornitz, D.M. (2008). An FGF-WNT gene regulatory network controls lung mesenchyme development. Dev. Biol. *319*, 426–436. https://doi.org/10.1016/j.ydbio.2008.04.009.

81. Zhang, X., Stappenbeck, T.S., White, A.C., Lavine, K.J., Gordon, J.I., and Ornitz, D.M. (2006). Reciprocal epithelial-mesenchymal FGF signaling is required for cecal development. Development *133*, 173–180. https://doi.org/10.1242/dev.02175.

82. Tribioli, C., Frasch, M., and Lufkin, T. (1997). Bapx1: an evolutionary conserved homologue of the Drosophila bagpipe homeobox gene is expressed in splanchnic

mesoderm and the embryonic skeleton. Mech. Dev. *65*, 145–162.

83. Kanzler, B., and Dear, T.N. (2001). Hox11 acts cell autonomously in spleen development and its absence results in altered cell fate of mesenchymal spleen precursors. Dev. Biol. *234*, 231–243. https://doi.org/10.1006/dbio.2001.0239.

84. Yin, Y., and Ornitz, D.M. (2020). FGF9 and FGF10 activate distinct signaling pathways to direct lung epithelial specification and branching. Sci. Signal. *13*, eaay4353. https://doi.org/10.1126/scisignal.aay4353.

85. Trapnell, C., Pachter, L., and Salzberg, S.L. (2009). TopHat: discovering splice junctions with RNA-Seq. Bioinformatics *25*, 1105–1111. https://doi.org/10.1093/bioinformatics/btp120.

86. Anders, S., Pyl, P.T., and Huber, W. (2015). HTSeq — a Python framework to work with high-throughput sequencing data. Bioinformatics *31*, 166–169. https://doi.org/10.1093/bioinformatics/btu638.

87. Schneider, C.A., Rasband, W.S., and Eliceiri, K.W. (2012). NIH Image to ImageJ: 25 years of image analysis. Nat. Methods *9*, 671–675. https://doi.org/10.1038/nmeth.2089.

88. Love, M.I., Huber, W., and Anders, S. (2014). Moderated estimation of fold change and dispersion for RNA-seq data with DESeq2. Genome Biol. *15*, 550. https://doi.org/10.1186/s13059-014-0550-8.

89. Stuart, T., Butler, A., Hoffman, P., Hafemeister, C., Papalexi, E., Mauck, W.M., Hao, Y., Stoeckius, M., Smibert, P., and Satija, R. (2019). Comprehensive integration of single-cell data. Cell *177*, 1888–1902.e21. https://doi.org/10.1016/j.cell.2019.05.031.

90. Kamburov, A., Pentchev, K., Galicka, H., Wierling, C., Lehrach, H., and Herwig, R. (2011). ConsensusPathDB: toward a more complete picture of cell biology. Nucleic Acids Res. *39*, D712–D717. https://doi.org/10.1093/nar/gkq1156.

STAR★METHODS

KEY RESOURCES TABLE

REAGENT or RESOURCE	SOURCE	IDENTIFIER
Antibodies		
Guinea Pig Polyclonal Anti-Pdx1	Abcam	Cat#ab47308
Rat Monoclonal Anti-Epcam	BD Pharmingen	Cat#552370
Rabbit Monoclonal Anti-Vimentin	Abcam	Cat#ab92547
Chicken Polyclonal Anti-Vimentin	Abcam	Cat#ab24525
Rat Monoclonal Anti-CD31	BD Pharmingen	Cat#553370
Guinea Pig Polyclonal Anti-Glucagon	MilliporeSigma	Cat#4031-01F
Guinea Pig Polyclonal Anti-Insulin	Dako	Cat#A0564
Goat Polyclonal Anti-Somatostatin	Santa Cruz Biotechnology	Cat#sc-7819
Goat Polyclonal Anti-Ghrelin	Santa Cruz Biotechnology	Cat#sc-10368
Goat Polyclonal Anti-Pancreatic polypeptide	Abcam	Cat#ab77192
Rabbit Polyclonal Anti-Cleaved caspase-3	Cell Signaling Technology	Cat#9661
Rabbit Polyclonal Anti-Collagen IV	Abcam	Cat#ab6586
Rabbit Monoclonal Anti-Wt1	Abcam	Cat#ab89901
Rabbit Polyclonal Anti-Laminin	MilliporeSigma	Cat#L9393
Anti-Cytokeratin 19	Abcam	Cat#ab133496
Goat Polyclonal Anti-Cpa1	R&D Systems	Cat#AF2765
Monoclonal Mouse Anti-Tuj1	R&D Systems	Cat#MAB1195
Goat Polyclonal Anti-Sma	Abcam	Cat#Ab21027
Mouse Monoclonal Anti-E-cadherin	BD Biosciences	Cat#610182
Rabbit Polyclonal Anti-Chga	Abcam	Cat#ab15160
Goat Polyclonal Anti-Pdx11	R&D Systems	Cat#AF2419
Rabbit Monoclonal Anti-Cytokeratin 19 (KRT19)	Abcam	Cat#Ab76539
Chemicals, peptides, and recombinant proteins		
In situ probe against mouse *Gcg*	Advanced Cell Diagnostics, Inc.	Cat#400601
In situ probe against mouse *Ins*	Advanced Cell Diagnostics, Inc.	Cat#414661
In situ probe against mouse *Ngn3*	Advanced Cell Diagnostics, Inc.	Cat#422401
In situ probe against mouse *Fev*	Advanced Cell Diagnostics, Inc	Cat#413241
In situ probe against mouse *Fgf9*	Advanced Cell Diagnostics, Inc.	Cat#499811
In situ probe against mouse *Fgf10*	Advanced Cell Diagnostics, Inc.	Cat#446371
In situ probe against mouse *Fgfr1*	Advanced Cell Diagnostics, Inc.	Cat#454941
In situ probe against mouse *Fgfr2*	Advanced Cell Diagnostics, Inc.	Cat#443501
In situ probe against mouse *Fgfr3*	Advanced Cell Diagnostics, Inc.	Cat#444101
In situ probe against mouse *Barx1*	Advanced Cell Diagnostics, Inc.	Cat#414681
In situ probe against mouse *Mgp*	Advanced Cell Diagnostics, Inc.	Cat#463381
In situ probe against mouse *Gap43*	Advanced Cell Diagnostics, Inc.	Cat#318621
In situ probe against human *FGF9*	Advanced Cell Diagnostics, Inc.	Cat#422421
In situ probe against human *FGFR1*	Advanced Cell Diagnostics, Inc.	Cat#310071
In situ probe against human *FGFR2*	Advanced Cell Diagnostics, Inc.	Cat#311171
In situ probe against human *FGFR3*	Advanced Cell Diagnostics, Inc.	Cat#310791
In situ probe against human *FGFR4*	Advanced Cell Diagnostics, Inc.	Cat#443439
In situ probe against human *WT1*	Advanced Cell Diagnostics, Inc.	Cat#415581

(*Continued on next page*)

Continued

REAGENT or RESOURCE	SOURCE	IDENTIFIER
Critical commercial assays		
RNAscope Muliplex Fluorescence Reagent Kit v2	Advanced Cell Diagnostics, Inc.	Cat#323110
Direct-zol RNA Microprep Kit	Zymo Research	Cat#R2060
NEBNext Ultra II RNA Library Prep Kit for Illumina version 1.0	New England Biolabs	Cat#E7770S
Chromium Single Cell 3′ Reagent Version 3.1 Kit	10x Genomics	Cat#PN-1000128
Click-iT EdU Alexa Fluor 555 Imaging Kit	Invitrogen	Cat#C10338
Deposited data		
Raw and processed single-cell sequencing data of Fgf9 null and control mouse pancreas tissue	This paper	GEO: GSE210645
Raw and processed bulk RNA-sequencing data of Fgf9 null and control pancreas tissue	This paper	GEO: GSE210574
Experimental models: Organisms/strains		
Mouse: *Fgf9*^{lacZ}	Huh et al.[49]	N/A
Mouse: C57BL/6J	The Jackson Laboratory	JAX: 000664
Software and algorithms		
TopHat	Trapnell et al.[85]	https://ccb.jhu.edu/software/tophat/index.shtml
HTSeq	Anders et al.[86]	https://htseq.readthedocs.io/en/master/
ImageJ	Schneider et al.[87]	https://imagej.nih.gov/ij/
DESeq2	Love et al.[88]	https://bioconductor.org/packages/release/bioc/html/DESeq2.html
ConsensusPathDB	Kamburov et al.[88]	http://cpdb.molgen.mpg.de/
CellRanger Count v.6.1.1	10x Genomics	https://support.10xgenomics.com/single-cell-gene-expression/software/downloads/latest
CellFindR	Yu et al.[70]	https://github.com/kevyu27/CellFindR
CellChat	Jin et al.[72]	https://github.com/sqjin/CellChat
Seurat v3.2.3	Stuart et al.[89]	https://github.com/satijalab/seurat
Prism 8 software	GraphPad	https://www.graphpad.com/scientific-software/prism/

RESOURCE AVAILABILITY

Lead contact

Further information and requests for resources and reagents should be directed to the lead contact and corresponding author, Julie B. Sneddon (Julie.Sneddon@ucsf.edu).

Materials availability

All unique/stable reagents generated in this study are available from the corresponding author with a completed Materials Transfer Agreement.

Data and code availability

- Raw and processed single-cell sequencing data of *Fgf9* null and control mouse pancreas samples have been deposited at GEO. Accession numbers are listed in the key resources table. These data are publicly available as of the date of publication.
- This paper does not report original code.
- Any additional information required to reanalyze the data reported in this paper is available from the lead contact upon request.

EXPERIMENTAL MODEL AND SUBJECT DETAILS

Animals

Fgf9-lacZ mice have been previously described.[49] Mice were maintained on a C57BL/6J background. Wild-type C57BL/6J mice were obtained from Jackson Laboratory. For timed matings, noon of the day of a vaginal plug was considered embryonic day (E)0.5. All mouse procedures were approved by the University of California, San Francisco (UCSF) Institutional Animal Care and Use Committee (IACUC). A range of developmental stages was used, from E10.5 to E17.5, and both male and female embryos were used.

METHOD DETAILS

Histology, immunofluorescence, and imaging of mouse tissue

Entire mouse embryos (for staining at E12.5 and earlier) or individual embryonic pancreata were dissected in ice cold PBS, photographed, weighed, and then fixed in 4% paraformaldehyde (PFA) for 30 to 90 minutes at room temperature (RT) or overnight at 4°C. After three washes in PBS, tissue was preserved in 30% sucrose in PBS at 4°C overnight and then embedded in Optimal Cutting Temperature (O.C.T.) compound (Tissue-Tek) and flash frozen prior to sectioning at 8 μm.

For immunofluorescence, cryosections were washed 3 times in PBS, permeabilized in 0.5% triton X-100 in PBS (PBT) for 10 minutes at RT, and then blocked with 5% normal donkey serum (NDS) in 0.1% PBT for 1 hour. Sections of mouse pancreas were stained overnight at 4°C using primary antibodies against Pdx1 (1:200, Abcam ab47308), Epcam (1:200, BD Pharmingen 552370), Vimentin (1:200, Abcam ab92547 or ab24525), CD31 (1:200, BD Pharmingen 553370), Glucagon (1:2000, MilliporeSigma 4031-01F), Insulin (1:250, Dako A0564), Somatostatin (1:500, Santa Cruz Biotechnology sc-7819), Ghrelin (1:1500, Santa Cruz Biotechnology sc-10368), Pancreatic Polypeptide (PPY; 1:250, Abcam ab77192), Cleaved Caspase-3 (1:200, Cell Signaling Technology, #9661), Collagen IV (1:200, Abcam, ab6586), Wt1 (1:200, Abcam, ab89901), Laminin (1:100, MilliporeSigma, L9393), Cytokeratin 19 (1:100, Abcam, ab133496), Cpa1 (1:100, R&D Systems AF2765), Class III Beta-Tubulin (TuJ1; 1:100, R&D Systems, MAB1195), Sma (1:250, Abcam, ab21027), E-Cadherin (1:100, BD Biosciences, 610182), and Chga (1:250, Abcam, ab15160).

The next day, sections were washed three times in PBS and then incubated with species-specific Alexa Fluor 488-, 555-, 594-, or 647-conjugated secondary antibodies and DAPI in 5% NDS in 0.1% PBT for 1 hour at RT. Sections were washed three times in PBS and covered in Fluoromount-G mounting medium. Images were captured on an SP8 Leica confocal laser scanning microscope. Maximum intensity z-projections were then prepared using ImageJ software.[87] To calculate the mean E11.5 mesenchyme tissue area as percent of the total area of mesenchyme and epithelium, three to four 20x fields were counted for each embryo, and sections from three embryos were analyzed for both control and *Fgf9* null groups. Epithelial area was defined as the region stained by antibody against Pdx1. Mesenchymal area was defined as the region stained by antibody against Vimentin and not stained by antibody against Pdx1. ImageJ software was used to measure tissue areas.

Whole-mount staining

Gut tubes were dissected from E11.5 and E13.5 mouse embryos and fixed at 4°C for 45 minutes in 4% PFA. After three washes in PBS, tissue was incubated in 0.5% PBT overnight, then blocked in 10% NDS in 0.1% PBT for 3 days at 4°C. E13.5 tissues were stained for four days at 4°C in primary antibody against EpCAM (1:100, BD Pharmingen 552370), and E11.5 tissues were stained for two days at 4°C in primary antibodies against EpCAM (1:100, BD Pharmingen 552370) and Pdx1 (1:200, Abcam ab47308). After three washes in PBS, tissue was incubated in secondary antibodies as above for two days, then washed again in PBS prior to placing in Ce3D Tissue Clearing Solution (BioLegend, 427703) for three days prior to imaging on an SP8 confocal microscope using a 10x objective.

Histology, immunofluorescence, and staining of human tissue

Informed consent was obtained for all human tissue collection, and protocols were approved by the Human Research Protection Program Committee at UCSF. Human fetal dorsal pancreas tissue was obtained from post-mortem fetuses at nine weeks post conception (wpc) through two sources: University of Washington Birth Defects Research Laboratory and Advanced Bioscience Resources, Inc. Identifiers were maintained at the source only, and the investigators received only de-identified specimens. After isolation, tissue was shipped overnight on ice in RPMI medium. Tissue was fixed in 4% PFA overnight at 4°C, washed three times

with PBS, and cryopreserved in 30% sucrose solution at 4°C overnight in preparation for embedding in O.C.T. compound. Sections measuring 10 μm in thickness were cut using a cryostat and stored at -80°C for multiplexed immunofluorescence staining and *in situ* hybridization, as described below.

Immunofluorescence staining on human tissue was performed as described above for mouse tissue, but using the following antibodies: Pancreatic and duodenal homeobox 1 (PDX1; 1:100, R&D Systems, AF2419), Cytokeratin 19 (KRT19; 1:100, Abcam, ab76539), Vimentin (VIM; 1:200, Abcam, ab24525), and E-Cadherin (E-CAD; 1:100, BD Transduction Laboratories, 610182).

In situ hybridization

In situ hybridization was performed on 8 μm thick cryosections of mouse embryonic pancreas using RNAscope technology (Advanced Cell Diagnostics, Inc.) according to the manufacturer's instructions. *In situ* probes against mouse *Gcg* (#400601), *Ins* (#414661), *Ngn3* (#422401), *Fev* (#413241), *Fgf9* (#499811), *Fgf10* (#446371), *Fgfr1* (#454941), *Fgfr2* (#443501), *Fgfr3* (#444101), *Barx1* (#414681), *Mgp* (#463381), and *Gap43* (#318621) were used with the RNAscope Multiplex Fluorescent Reagent Kit v2 for target transcript detection. Following signal amplification of the target probes, sections were washed in PBS three times prior to proceeding to blocking steps, antibody staining, and imaging as described above.

In situ hybridization was also performed in similar fashion on 10 μm thick cryosections of human fetal dorsal pancreas tissue, using *in situ* probes against human *FGF9* (#422421), *FGFR1* (#310071), *FGFR2* (#311171), *FGFR33* (#310791), *FGFR4* (#443439), and *WT1* (#415581).

Bulk RNA-Sequencing and analysis

For bulk RNA-Sequencing at E13.5, three independent replicates were performed. For Replicate 1, 12 pancreata from control embryos (including $Fgf9^{LacZ/+}$ and $Fgf9^{+/+}$) were pooled, and seven null pancreata from *Fgf9* null embryos were pooled, from two litters. For Replicate 2, seven control pancreata from one litter were pooled, and six null pancreata were pooled from two litters. For Replicate 3, 12 control pancreata were pooled from one litter (and no null embryos were obtained for this third replicate).

For bulk RNA-Sequencing at E14.5, three independent replicates were also performed. For Replicate 1, eight pancreata from control embryos (including $Fgf9^{LacZ+/+}$ and $Fgf9^{+/+}$) were pooled from one litter, and four null embryos from two litters were pooled. For Replicate 2, seven control pancreata were pooled from one litter, and three null pancreata were pooled from two litters. For Replicate 3, six control pancreata were pooled from one litter (no null embryos were obtained for this third replicate). Classification as null was initially based on the appearance of a hypoplastic spleen, with later confirmation by genotyping.

Pancreata were dissected in ice cold PBS from E13.5 and E14.5 murine embryos and immediately placed in TRIzol Reagent (Invitrogen, 15596026). Total RNA was extracted using Direct-zol RNA Microprep Kits (Zymo Research, R2060) according to the manufacturer's instructions. Total RNA was submitted to Novogene for library preparation and sequencing. Library preparation was performed using the NEBNext Ultra II RNA library Prep Kit for Illumina version 1.0 (NEB), following manufacturer's instructions for the NEBNext Poly(A) mRNA Magnetic Isolation Module (NEB, #E7490).

Sequencing was performed on the Illumina NovaSeq 6000 platform. Sequencing reads were then mapped to the reference genome (mm10) using TopHat[85] and transcript counts were quantified with HTSeq.[86] Differential gene expression analysis was performed using DESeq2.[88] Pathway analysis was performed using ConsensusPathDB[90] with an overrepresentation test.

Preparation of tissue for single-cell RNA-Sequencing

E14.5 pancreata were dissected and placed in PBS on ice. Pancreata from *Fgf9* null and control mice were distinguished by their morphological appearance, and later validated by genotyping. Three *Fgf9* null pancreata from three litters were pooled, and eight control pancreata from three litters were pooled. Pancreata were minced into small pieces and dissociated into single cells using TrypLE Express dissociation reagent at 37°C for 15 min. Dissociations were neutralized with FACS buffer (10% FBS+ 2 mM EDTA in phenol-red free HBSS), and cell suspensions were passed through 30 μm cell strainers. Single cells were stained with DAPI (10 μg/mL) before loading onto a BD FACSAria II cell sorter (BD Biosciences). After size selection to

remove doublets, all DAPI negative (live) cells were collected. The number and viability of sorted cells were examined using the Countess II automated cell counter (ThermoFisher).

Mouse single-cell capture and sequencing

For scRNA-Seq of embryonic mouse pancreas, we used the Chromium Single Cell 3′ Reagent Version 3.1 Kit (10x Genomics). 25,000 live cells from pooled control pancreata and 25,000 live cells from pooled *Fgf9* null pancreata were loaded onto separate lanes of a single 10x chip. Gel Bead-In EMulsions (GEMs) were generated and subjected to reverse transcription for RNA barcoding before cleanup and cDNA amplification. Libraries were then prepared according to the manufacturer's instructions (10x Genomics). Each resulting library was sequenced on the Novaseq 6000 platform (Illumina) using the S4 flowcell with the following parameters: Read 1 – 28 cycles, Index 1 i7 – 8 cycles, Index 2 i5 – 0 cycles, Read 2 – 91 cycles.

Analysis of mouse single-cell RNA-Sequencing data

To assemble the transcriptomic profiles of individual cells, we utilized CellRanger Count v.6.1.1 with default settings to demultiplex, aligned reads to the murine genome (mm10, supplied by 10x Genomics), and quantified unique molecular identifiers (UMIs). The resulting gene-barcode matrices were then analyzed and merged with the R package Seurat v3.2.3.[89] High-quality cells were retained by filtering on the number of expressed genes and mitochondrial content. Each sample was normalized with NormalizeData(), and variable genes were identified with the FindVariableFeatures() function using 2,000 genes and the "vst" selection method. Integration anchors were found across all samples with the FindIntegrationAnchors() with 30 principal components and 2,000 genes. The samples were then integrated using the IntegrateData() function. The data was then scaled with ScaleData() function and principal component analysis (PCA) was performed, with 30 principal components selected based on the ElbowPlot(). Dimensionality reduction and initial clustering was performed with the FindNeighbors(), FindClusters() and RunUMAP() functions using 30 principal components and a resolution parameter of 0.2. The resulting clusters were then annotated into Broad Groups based on expression of known markers for each respective Broad Group (e.g. *Col3a1*+ mesenchymal cells).

To further sub-cluster the Broad Groups, we applied the clustering package CellFindR (https://github.com/kevyu27/CellFindR).[70] Each Broad Group was individually subsetted, PCA and UMAP were recalculated, and the top level resolution was found with the res() function. Iterative sub-clustering was performed on each top level cluster with the sub_clustering() function. Clusters that were deemed non-biological were manually removed. Cell types were then annotated, when possible, based on expression of either known or novel marker genes.

Differentially expressed genes (DEGs) of each CellFindR cluster in the merged dataset were identified with Seurat FindAllMarker() function. The DEGs between control and *Fgf9* null genotype of a given CellFindR cluster were calculated by EnhancedVolcano() function. Pathway analysis was performed using ConsensusPathDB[90] with an overrepresentation test.

Analysis of human single-cell RNA-Sequencing data

Generation of the human fetal single-cell RNA-Sequencing dataset, including processing of pancreas tissue, single-cell capture and sequencing, and single-cell RNA-Sequencing analysis, were performed previously as described.[73] Pathway analysis was performed using ConsensusPathDB[90] with an overrepresentation test.

Quantification of pancreatic cellular communication with CellChat

We utilized the R package CellChat[72] (https://github.com/sqjin/CellChat) to perform cellular signaling analysis in the developing murine pancreas and the developing human fetal pancreas.

QUANTIFICATION AND STATISTICAL ANALYSIS

Quantification of PDX1+ cells in dorsal pancreas

Immunofluorescence was performed on E10.5 tissue from control and *Fgf9* null pancreata to stain for PDX1 to mark pancreatic progenitor cells at this early developmental stage. The number of PDX1+ cells within the dorsal pancreas of each 8 μm section was manually counted using ImageJ software. A total of 20 control sections from five embryos and 18 *Fgf9* null sections from five embryos were quantified. Each individual

embryo is represented by a single data point. Error bars represent standard deviation, and significance was assessed using two-tailed nested t-test.

Analysis of cellular proliferation

Pregnant female mice were injected with 5-Ethynyl-2-deoxyuridine (EdU) at a dose of 50 μg/g of body weight. Time of incubation prior to sacrifice depended on embryonic age: 30 minutes for E10.5, 1 hour for E11.5, and 2 hours for E12.5 and older. Embryos were dissected in ice cold PBS, processed, and sectioned as above. For EdU detection, the Click-iT™ EdU Alexa Fluor™ 555 Imaging Kit (Invitrogen) was used per manufacturer's instructions prior to proceeding to blocking steps, antibody staining, and imaging as described above. Proliferation index was calculated as the fraction of total nuclei that were EdU-labeled in fields captured by a 20x objective.

The percentage of Pdx1+EdU+ cells within all Pdx1+ pancreatic progenitor cells from control and *Fgf9* null pancreatic tissues were counted manually in ImageJ. A total of 17 control sections from four embryos and 13 *Fgf9* null sections from four embryos were used for quantification at E10.5. Each individual embryo is represented by a single data point. Error bars represent standard deviation, and significance was assessed using two-tailed nested t-test. Proliferative index of Pdx1+ epithelial cells and Pdx1- mesenchymal cells was quantified for *Fgf9* null and control sections at E11.5 (n = 4 control pancreata, n = 3 null pancreata). Proliferative index of Epcam+ epithelial cells and Epcam- mesenchymal cells was quantified for *Fgf9* null and control sections at E12.5 (n = 3 control pancreata, n = 3 null pancreata) and E14.5 (n = 3 control pancreata, n = 3 null pancreata), respectively. Each individual embryo is represented by a single data point. Error bars represent standard deviation, and significance was assessed using two-tailed nested t-test.

Quantification and statistical analysis of endocrine populations

To assess the proportional changes in cell populations within the endocrine compartment, three control pancreata and two *Fgf9* null pancreata from the same E14.5 litter were subjected to multiplexed staining with RNAscope probes against *Ins, Gcg, Fev,* or *Neurog3* in a single experimental batch. Confocal (Leica SP8) images were taken for 19 randomly chosen regions of interest in sections of the three control pancreata and for 25 randomly chosen regions of interest in sections of the two *Fgf9* null pancreata. Annotation of cells as positive for *Ins, Gcg, Fev,* and/or *Neurog3* and quantification was performed manually with ImageJ software[87] using the cell counter plug-in. For each image, the proportion of each cell state present was then calculated using the sum of cells corresponding to all annotated cell states as the denominator, and cells that scored positive for a given cell state as the numerator.

Data were presented as mean ± standard deviation, and differences in cell proportion between control and *Fgf9* null tissue were determined with an unpaired t-test using GraphPad software (Prism 8).